

A Random Rule Model

Avner Seror*

March 19, 2026

Abstract

We study stochastic choice when behavior is generated by switching among a small library of transparent deterministic decision procedures. The object of interest is procedural heterogeneity: how the relative importance of these procedures varies across decision environments. We model this heterogeneity with a Random Rule Model (RRM), in which menu-level choice probabilities arise from environment-dependent weights on named rules. We show that identification has a two-step structure. At a fixed feature value, variation in decisive-side patterns across menus identifies the vector of relative rule weights up to scale; across sufficiently rich feature values, these recovered weights identify the parameters of an affine gate. Applied to a large dataset of binary lottery choices, the estimated procedure weights are concentrated on a small subset of interpretable rules and shift systematically with menu characteristics such as tradeoff complexity and dispersion asymmetry. Out-of-sample prediction and cross-dataset portability provide supporting evidence that the recovered procedural representation is empirically disciplined.

Keywords: Behavioral Economics, Decision Theory, Random Rule Model, Identification, Risky Choice, Machine Learning.

JEL Classification: D81, C25, C52, D91.

1 Introduction

Stochastic choice data are often interpreted through latent utility heterogeneity, random utility shocks, or menu-dependent consideration. An alternative possibility is that observed choice frequencies reflect systematic switching across decision procedures. In many environments, agents may sometimes screen on extreme outcomes, sometimes compare modal consequences, sometimes focus on salient payoff differences, and sometimes follow simpler attention-based procedures. The central object in such settings is not only the average choice probability attached to a menu, but the procedural heterogeneity that determines which decision procedures are more prevalent in which environments.

*Aix-Marseille University, CNRS, AMSE, Marseille, France. Email: avner.seror@univ-amu.fr. I am grateful to Marina Agranov, Benjamin Enke, En Hua Hu, Dotan Persitz, John Quah, and Thierry Verdier for helpful discussions. I acknowledge funding from the French government under the ANR JCJC “BIAS” project (reference: ANR-25-CE26-7164-01) and the “France 2030” investment plan managed by the French National Research Agency (reference: ANR-17-EURE-0020) and from the Excellence Initiative of Aix-Marseille University – A*MIDEX. Mistakes are my own. Parts of this manuscript were prepared with the assistance of large language models (Claude and GPT). Refine.ink was used to check the paper for consistency and clarity. The author used these tools for code development and editorial revisions; all scientific content, modeling choices, and results were produced and verified by the author.

This paper studies stochastic choice through that lens. We develop a Random Rule Model (RRM) in which behavior is generated by random switching among a small library of transparent, deterministic decision rules. Each rule maps a menu into a recommendation; stochastic choice arises because the relative weight placed on these rules varies with observable features of the menu. The resulting model yields an explicit procedural decomposition of behavior: changes in choice frequencies across environments are interpreted as changes in the prevalence of named lines of conduct rather than as shifts in an unobserved reduced-form predictor.

This representation is attractive for several reasons. First, it provides a tractable language for procedural heterogeneity in large choice environments. Rather than forcing a single valuation model to govern all menus, the model allows different procedures to matter in different regions of the environment space. Second, it remains economically interpretable: the primitive objects are transparent rules with clear behavioral content. Third, it imposes discipline. The model can fit choice frequencies only through the patterns of agreement and disagreement generated by the rule library and through systematic variation in the corresponding rule weights. Fourth, it does not require transitivity or other consistency conditions on the aggregate choice function: because each rule is applied independently and the mixture weights vary freely with menu features, the model can accommodate systematic violations of classical rationality axioms that are well-documented in stochastic choice data.

The rule weights depend on observable features of the menu, and not all rules deliver a strict recommendation on every menu - the model restricts behavioral responsibility to rules that are actually decisive, ensuring that the decomposition attributes weight only where a rule provides a clear-cut ranking. The formal mechanism is a softmax gate over rule-specific indices.

The main theoretical question is whether the latent procedural weights are genuinely identified from menu-level choice frequencies. We show that they are, under a two-layer structure. In the first layer, consider menus that share the same value of the feature vector used by the gate (a possibly coarsened summary of the full menu description). These menus also share the same latent rule weights, but they may differ in which rules recommend which option — some rules switch sides across menus even when the gate features are held fixed. This rule-switching variation pins down the relative importance of the rules at a given set of characteristics: if enough rules switch sides across enough menus, the data uniquely determine how much weight each rule carries. In the second layer, once relative rule weights have been recovered at sufficiently many distinct menu characteristics, the law governing how those weights change with menu features is itself identified. Global identification thus separates cleanly into a within-characteristic step that uses rule switching to recover relative weights, and an across-characteristic step that maps those weights back into the gate.

The identification theorem is constructive: it implies a two-step estimator in which normalized rule weights are first recovered cell by cell from the linear restrictions generated by rule switching, and the gate parameters are then estimated from the cross-cell variation in recovered log-weights. We establish consistency and asymptotic normality for this estimator, yielding inference for economically meaningful functionals of the decomposition.

For the main empirical analysis, however, we estimate the model by minimizing out-of-sample mean squared error (MSE). This avoids the binning of the feature space into discrete cells that the two-step procedure requires and places the rule-gating model on the same predictive footing as the neural-network benchmarks against which it is evaluated. The cellwise identification theory guarantees that the rule weights recovered at each menu characteristic have structural content

— they are pinned down by the data, not merely by the predictive objective. When the gate specification is correct, both estimators target the same population decomposition; the two-step estimator provides a built-in diagnostic for this restriction.

We apply the framework to the `choices13k` dataset of Peterson et al. (2021), which contains thousands of distinct binary lottery menus with repeated observations per menu. We construct a library of twelve parameter-free decision rules spanning canonical behavioral mechanisms — extreme-outcome screening, modal-outcome comparisons, salience-based comparisons, regret- and disappointment-type comparisons, and limited-consideration-style defaults — and estimate the model using the same cross-validation protocol as Peterson et al. (2021). We first verify the identification conditions on the data, then report the MSE-fitted behavioral decomposition: responsibility weights (the average share of predicted choice attributed to each rule), ablation indices (the predictive deterioration when a rule is removed), and concentration measures (how dispersed rule usage is across the library). The two-step econometric estimates follow as a cross-check. We then study how rule responsibility shifts with interpretable menu characteristics such as tradeoff complexity and dispersion asymmetry, and conclude with predictive validation and portability to an independent dataset.

The main empirical findings are as follows. First, on identification: both conditions of the global identification theorem are satisfied on the Choices13k data, with rule rankings by responsibility weight highly stable across training samples and ablation rankings moderately stable. Second, on the behavioral decomposition: the attention channel (left/right defaults) absorbs roughly half of effective responsibility, consistent with substantial inattention in online data collection. Among the structured rules, salience-based comparisons, regret-type comparisons, and modal-outcome screening carry the largest non-attention shares. Ablations are even more selective: removing either salience-based comparison produces the largest deterioration in MSE, followed by regret-type comparisons, extreme-max screening, and modal-outcome comparisons, whereas disappointment-type procedures and the modal-average rule contribute little or negative incremental content. Rule responsibility shifts systematically with objective menu primitives. Along tradeoff complexity, regret shows the steepest decline, the mixture reallocates toward attention and salience-based comparisons, and modal-outcome comparisons weaken, consistent with the view that decision-makers facing more complex tradeoffs fall back on simpler heuristics or default behavior. Along dispersion asymmetry, regret declines steeply while attention defaults rise, suggesting that large differences in spread push the gate toward simpler default behavior.

Third, on predictive performance: in out-of-sample evaluation, rule-gating (MSE 0.0117) substantially outperforms neural-network implementations of expected utility (0.0222), prospect theory (0.0206), and cumulative prospect theory (0.0215), as well as a value-based network (0.0192), and outperforms a flexible context-dependent neural predictor (0.0134). Only the Mixture of Theories (MOT, 0.0114), a mixture-of-experts architecture from Peterson et al. (2021), achieves lower MSE. Rule-gating closes about 97% of the Neural-EU-to-MOT gap. Moreover, rule-gating outperforms MOT at small-to-moderate training fractions; MOT’s advantage emerges only with large samples, consistent with its larger number of free parameters requiring more data to pay off.

Fourth, on restrictiveness and portability: a permutation-fit diagnostic reveals that rule-gating is essentially fully restrictive — when trained on randomly permuted choice frequencies, it does no better than a constant predictor, meaning the model cannot absorb structureless variation. MOT, by contrast, fits permuted targets about five times better than a constant predictor, indicating substantial capacity to absorb structureless variation. This distinction is confirmed by out-of-sample

portability: we export all models — without re-tuning — to the Choice Prediction Competition 2018 (CPC18) dataset (Erev et al., 2017; Plonsky et al., 2017), an independent collection of binary lottery choices with different subjects and a different menu sample. Rule-gating and the context-dependent model transfer well, far ahead of the structured benchmarks, while MOT deteriorates sharply.

We subject the framework to a battery of robustness checks addressing library composition, the attention channel, the activity discipline, and the choice of gate features. Cross-fitted library selection retains the bulk of accuracy with 7 rules, and the selected rules coincide with those receiving the highest responsibility weights. Removing the two attention rules brings MSE to 0.0201, still close to or outperforming most structured benchmarks. Varying the activity discipline reveals that over-restricting the activity set is more costly than removing it, so the dominance-based activation is best understood as an interpretive discipline rather than a predictive one. A placebo test, in which rule indicators are randomly reassigned across menus while preserving their marginal statistics, confirms that the rule indicators carry genuine, menu-specific predictive content: the gate’s performance depends on the structured correspondence between menus and rule recommendations, not merely on the availability of additional binary regressors. Finally, an interpretable twelve-dimensional vector of summary statistics performs as well as a higher-dimensional raw menu encoding as gate input, indicating that the economically motivated features capture the decision-relevant variation without overfitting.

Related literature. Our approach relates to the literature on stochastic choice. In random utility models (RUM), choice probabilities are generated by heterogeneity in latent utilities (McFadden, 2006; McFadden and Richter, 1991; Kitamura and Stoye, 2018). A related literature accounts for limited, random, or menu-dependent consideration, jointly recovering preferences and attention/consideration mechanisms from stochastic choice data (Manzini and Mariotti, 2014; Cattaneo et al., 2020; Aguiar et al., 2023). The RRM adopts a different primitive: stochasticity operates through randomization over a small library of interpretable decision procedures rather than through random utilities or random consideration sets. It should be viewed as a procedural stochastic-choice model that is generally neither nested in, nor nests, the RUM and attention frameworks.

Our identification argument connects to the econometrics of latent heterogeneity. The first-stage identification — recovering mixture weights from linear restrictions generated by rule switching — is structurally related to identification in finite mixture models with instrument-like variation (Henry et al., 2014). The novelty is that the identifying variation comes from the discrete patterns of decisive-side recommendations, which are observable and deterministic, rather than from excluded instruments or panel structure.

The paper also connects to the broader tradition of modeling choice as the outcome of procedures under bounded rationality and simplicity constraints (Simon, 1955; Rubinstein, 1988; Aumann, 2008; Manzini and Mariotti, 2007, 2012; Cherepanov et al., 2013; Salant and Rubinstein, 2008), and to the behavioral literature on menu-dependent perception and evaluation (Kahneman and Tversky, 1979; Tversky and Kahneman, 1992; Bordalo et al., 2012; Loomes and Sugden, 1986; Masatlioglu et al., 2012). Our mechanism results relate to the literature on complexity and rule selection (Arrieta and Nielsen, 2024; Halevy and Mayraz, 2024; Puri, 2025; Enke and Shubatt, 2023); closest to our analysis, Enke and Shubatt (2023) construct menu-based complexity indices and show that “tradeoff complexity” predicts behavioral signatures in large-scale choice data. We build on this by studying how complexity and dispersion asymmetry are associated with systematic

reallocation of procedure weights inside an interpretable random-rule mixture. Our approach builds on the decision-rule primitives of Seror (2026); the present paper adds the gating mechanism, the identification theory, and the econometric framework.

Finally, our approach also speaks to the recent agenda of empirical machine learning in economics (Liang, 2025). Our completeness normalization follows recent work benchmarking economic structure against flexible ML baselines (e.g., Peysakhovich and Naecker, 2017; Fudenberg and Liang, 2020; Fudenberg and Puri, 2022; Fudenberg et al., 2022); our restrictiveness diagnostic applies the logic of Fudenberg et al. (2026); and we implement a portability exercise targeting external validity. Finally, a growing literature documents strong out-of-sample performance in risky choice (e.g., Erev et al., 2010, 2017; Plonsky et al., 2016; Peterson et al., 2021). Our contribution is to show that a disciplined mixture of interpretable procedures can recover a large share of these predictive gains while producing mechanism-level objects that are directly interpretable in economic terms.

2 Model

We develop the model and the identification theory for binary lottery menus, which is the setting of our empirical application. Appendix A presents the fully general framework covering arbitrary menu sizes, general dominance preorders, and multinomial choice. The two treatments share the same structure - a grouped-softmax representation, activity-conditional normalization, and verifiable conditions for global identification - with the main difference being notational: log-odds become log-ratios and two-sided menus become multi-sided menus. The binary exposition thus conveys the essential ideas with lighter notation.

2.1 Setup

A *menu* (choice set) is a binary set $A = \{L^1, L^2\}$ of lotteries, each lottery being a finite-support distribution over monetary outcomes. We label L^1 the left choice and L^2 the right choice. Let $\mathcal{A}_{\text{full}}$ denote the full set of menus in the dataset. Each $A \in \mathcal{A}_{\text{full}}$ is observed $n(A) \geq 1$ times. Let $c_m(A) \in \{L^1, L^2\}$ be the realized choice in repetition $m \in \{1, \dots, n(A)\}$. The menu-level left-choice frequency is

$$\hat{p}(A) := \frac{1}{n(A)} \sum_{m=1}^{n(A)} \mathbf{1}\{c_m(A) = L^1\} \in [0, 1].$$

We interpret $\hat{p}(A)$ as estimating a population choice probability $p(A) := \mathbb{P}(L^1 | A)$. A predictor is a function $g : \mathcal{A}_{\text{full}} \rightarrow [0, 1]$ intended to approximate $p(\cdot)$.

The dataset is a collection of observations $D = \{(c_t, A_t)\}_{t \in \mathcal{T}}$, where $\mathcal{T} := \{1, \dots, T\}$. The choice environment is characterized by the pair $((X, \succeq), \mathcal{A}_{\text{full}})$, where $\mathcal{A}_{\text{full}} = \{A_t\}_{t \in \mathcal{T}}$ and \succeq is a fixed dominance preorder on X . The statement $L^1 \succeq L^2$ means that L^1 is unambiguously perceived as better than L^2 according to the normative standard. We write \succ for the strict part of \succeq :

$$L^1 \succ L^2 \iff L^1 \succeq L^2 \text{ and not } (L^2 \succeq L^1).$$

We adopt First-Order Stochastic Dominance (FSD) as the dominance criterion.

Definition 1 (First-Order Stochastic Dominance). Let $L^1, L^2 \in X$. Let $\text{supp}(L^1) \cup \text{supp}(L^2) = \{z_1 < \dots < z_M\}$ be the ordered union of their supports. For $\ell \in \{1, 2\}$, let $\pi_k^\ell := \Pr_{L^\ell}(z_k)$ with the

convention $\pi_k^\ell = 0$ when $z_k \notin \text{supp}(L^\ell)$, and define the right-tail cumulative sums $S_i^\ell := \sum_{k=i}^M \pi_k^\ell$, $i = 1, \dots, M$. We say that $L^1 \geq_{\text{FSD}} L^2$ if and only if $S_i^1 \geq S_i^2$ for all $i = 1, \dots, M$. We denote the strict part by $>_{\text{FSD}}$.

Acts and States. For some of our decision rules introduced later, it is convenient to think of each lottery as induced by a state-contingent act. Formally, a choice problem can equivalently be described by a finite state space $S = \{1, \dots, n\}$, objective state probabilities $(p_s)_{s \in S}$, and, for each menu $A_t = \{L_t^1, L_t^2\}$, two acts corresponding to the two lotteries:

$$L_t^i \equiv (u_t^i(s))_{s \in S}, \quad u_t^i(s) \in \mathbb{R}.$$

Given $(p_s)_{s \in S}$, the act L_t^i induces a lottery representation $(z_t^i, \pi_t^i) \in X$ by grouping equal prizes and assigning to each distinct payoff its total probability:

$$\pi_{t,k}^i = \sum_{s \in S: u_t^i(s) = z_{t,k}^i} p_s.$$

The primitives of our model are lotteries, and all subsequent rules - including regret- and disappointment-type rules - are defined as functions of the lottery representation (or of a canonical state space constructed from the marginal distributions via the product measure over outcome pairs, as described in Section 4). Hence the lottery representation is without loss of generality for the properties we study: “without loss” is relative to the paper’s rule definitions, which take lottery representations as inputs, not joint state-act distributions.¹ We will use the state-space view only when defining several rules, and otherwise work with the simpler lottery notation introduced above.

2.2 Rule library and rule-induced perceived lotteries

We model behavior as the outcome of a small library of simple decision rules. Each rule provides a clear-cut line of conduct: it extracts a coarse feature of the menu, converts each option into a (perceived) lottery - often a sure outcome in our implementation - and then recommends the option that is superior according to FSD. For example, the decision rule can be “choose the option with the better worst-case outcome”.

We follow Seror (2026) in the characterization of rules below. Let \mathcal{F} be a finite collection of rules. Each rule maps a binary menu to a perceived binary menu:

$$f : X \times X \rightarrow X \times X, \quad f(L^1, L^2) = (\pi_f(L^1; L^2), \pi_f(L^2; L^1)),$$

where $\pi_f(L^i; L^j) \in X$ is a finite-support lottery. We evaluate perceived lotteries using the same dominance preorder as for objective lotteries; throughout the paper, \succeq is First-Order Stochastic Dominance (FSD).

For each menu $A = \{L^1, L^2\}$ and each rule $f \in \mathcal{F}$, define the *activity* and *left-recommendation* indicators

$$A_f(A) := \mathbf{1} \left\{ \pi_f(L^1; L^2) >_{\text{FSD}} \pi_f(L^2; L^1) \text{ or } \pi_f(L^2; L^1) >_{\text{FSD}} \pi_f(L^1; L^2) \right\}, \quad (1)$$

$$L_f(A) := \mathbf{1} \left\{ \pi_f(L^1; L^2) >_{\text{FSD}} \pi_f(L^2; L^1) \right\}. \quad (2)$$

¹For the regret- and disappointment-type rules, we construct a canonical state space from the product measure over outcome pairs of the two lotteries (Section 4). This coupling is a specific construction that does not invoke or require data on correlated state-act outcomes.

Thus $A_f(A) = 1$ means that rule f yields a *strict* dominance comparison in one direction (the rule is *decisive* at A), while $L_f(A) = 1$ means that, when decisive, it recommends choosing the left option.

Definition 2 (Activity). A rule $f \in \mathcal{F}$ is *active* at menu A if $A_f(A) = 1$, and *inactive* otherwise.

2.3 Conditional on Activity Random Rule Model (CA-RRM)

A Conditional on Activity Random Rule Model (CA-RRM) assigns to each menu A a vector $q(A) = \{q_f(A)\}_{f \in \mathcal{F}} \in \Delta^{F-1}$, where $q_f(A)$ is the propensity to apply rule f at A . Since not all rules are decisive at all menus, the model conditions on *activity*. We define the left mass and active mass:

$$\ell(A; q) = \sum_{f \in \mathcal{F}} q_f(A) L_f(A), \quad m(A; q) = \sum_{f \in \mathcal{F}} q_f(A) A_f(A).$$

The CA-RRM predicted left-choice probability is

$$g_{\text{CA}}(A) = \frac{\ell(A; q)}{\max\{m(A; q), m_{\min}\}} \in [0, 1], \quad (3)$$

where $m_{\min} > 0$ is a small guard constant to prevent numerical instability if the total active mass is near zero. In practice however, we have two ‘‘attention’’ rules in the library \mathcal{F} that can always be active, so $m(A; q)$ is typically strictly positive.

2.4 Rule-gating parameterization

CA-RRM becomes a *rule-gating predictor* when $q(A)$ is parameterized by a differentiable gate. Let $\psi(A) \in \mathbb{R}^d$ be a fixed-length encoding of the menu (defined precisely in Section 6.3). We use a softmax gate:

$$q_f(A; \theta) = \frac{\exp(\alpha_f + \beta_f^\top \psi(A))}{\sum_{g \in \mathcal{F}} \exp(\alpha_g + \beta_g^\top \psi(A))}, \quad (4)$$

where $\theta = \{(\alpha_f, \beta_f)\}_{f \in \mathcal{F}}$. The resulting predictor is $g_{\text{RG}}(A; \theta) = g_{\text{CA}}(A; q(\cdot; \theta))$ as in (3).

Combining (3) with (4), we have

$$g_{\text{RG}}(A; \theta) = \frac{\sum_{f \in \mathcal{F}} q_f(A; \theta) L_f(A)}{\sum_{f \in \mathcal{F}} q_f(A; \theta) A_f(A)} \quad (\text{up to the small guard } m_{\min}).$$

We define the *conditional-on-activity weights*

$$\tilde{q}_f(A; \theta) := \frac{q_f(A; \theta) A_f(A)}{\sum_{g \in \mathcal{F}} q_g(A; \theta) A_g(A)} \in [0, 1], \quad \sum_{f \in \mathcal{F}} \tilde{q}_f(A; \theta) = 1 \quad (5)$$

whenever the denominator is positive.² Then the CA-RRM prediction admits the simple mixture form

$$g_{\text{RG}}(A; \theta) = \sum_{f \in \mathcal{F}} \tilde{q}_f(A; \theta) L_f(A). \quad (6)$$

From (6), a CA-RRM operates as a mixture over deterministic rule recommendations, after filtering out rules that are inactive at A .

²In our implementation, rules A1 and A2 are always included and are decisive for essentially all menus, so the denominator is typically well away from zero.

3 Identification via Rule Switching

This section clarifies when the gate parameters $\theta = \{(\alpha_f, \beta_f)\}_{f \in \mathcal{F}}$ are pinned down by menu-level choice frequencies. The identification argument has two layers. The first layer identifies, at a fixed feature value, the vector of relative rule weights. The second layer uses variation across feature values to recover the affine gate parameters. The key identifying force throughout is *rule switching*: because different rules recommend different sides in different menus, the decisive-side pattern varies across the menu support, and this variation pins down the latent rule weights.

From CA-RRM to a collapsed binary logit index. For a menu $A = \{L^1, L^2\}$, define the decisive-left and decisive-right sets

$$\mathcal{I}_L(A) := \{f \in \mathcal{F} : A_f(A) = 1, L_f(A) = 1\}, \quad \mathcal{I}_R(A) := \{f \in \mathcal{F} : A_f(A) = 1, L_f(A) = 0\}.$$

Ignoring the numerical guard m_{\min} (inactive in our implementation), the softmax gate (4) combined with the CA normalization yields

$$g_{\text{RG}}(A; \theta) = \frac{\sum_{f \in \mathcal{I}_L(A)} \exp(\alpha_f + \beta_f^\top \psi(A))}{\sum_{f \in \mathcal{I}_L(A) \cup \mathcal{I}_R(A)} \exp(\alpha_f + \beta_f^\top \psi(A))}. \quad (7)$$

Define the inclusive values

$$V_L(A; \theta) := \log \sum_{f \in \mathcal{I}_L(A)} \exp(\alpha_f + \beta_f^\top \psi(A)), \quad V_R(A; \theta) := \log \sum_{f \in \mathcal{I}_R(A)} \exp(\alpha_f + \beta_f^\top \psi(A)).$$

Whenever $\mathcal{I}_L(A)$ and $\mathcal{I}_R(A)$ are both nonempty,

$$\log \frac{g_{\text{RG}}(A; \theta)}{1 - g_{\text{RG}}(A; \theta)} = V_L(A; \theta) - V_R(A; \theta). \quad (8)$$

Observed object. Let

$$\mathcal{A}_2 := \{A \in \mathcal{A}_{\text{full}} : \mathcal{I}_L(A) \neq \emptyset, \mathcal{I}_R(A) \neq \emptyset\}$$

denote the set of *two-sided* menus. For $A \in \mathcal{A}_2$, define the population log-odds

$$\delta(A) := \log \frac{p(A)}{1 - p(A)} = V_L(A; \theta) - V_R(A; \theta), \quad (9)$$

where $p(A) = \Pr(L^1 | A)$.

Normalization and parameter vector. Because the softmax gate is invariant to adding a common constant to all α_f and a common vector to all β_f , we impose a location normalization: fix one baseline rule $f_0 \in \mathcal{F}$ and set

$$(\alpha_{f_0}, \beta_{f_0}) = (0, 0). \quad (10)$$

Let $\vartheta \in \mathbb{R}^K$ collect the remaining free parameters, with

$$K = (|\mathcal{F}| - 1)(1 + \dim(\psi)).$$

Decisive-side indicators and the H matrix. For each rule f and menu A , define the decisive-side indicators

$$\kappa_f^L(A) := \mathbf{1}\{f \in \mathcal{I}_L(A)\}, \quad \kappa_f^R(A) := \mathbf{1}\{f \in \mathcal{I}_R(A)\},$$

and write the odds ratio

$$r(A) := \frac{p(A)}{1 - p(A)}.$$

For any $x \in \mathbb{R}^d$, define the positive weight vector

$$\omega_f(x) := \exp(\alpha_f + \beta_f^\top x).$$

Cross-multiplying the odds form of the model yields, for each menu A with $\psi(A) = x$,

$$\sum_{f \in \mathcal{F}} (\kappa_f^L(A) - r(A)\kappa_f^R(A)) \omega_f(x) = 0, \quad (11)$$

i.e. $h(A)^\top \omega(x) = 0$, where

$$h_f(A) := \kappa_f^L(A) - r(A)\kappa_f^R(A).$$

Identification in two layers. Equation (11) reveals the first identifying object: at a fixed feature value x , every menu with $\psi(A) = x$ shares the same latent weight vector $\omega(x)$, but may display a different decisive-side pattern. These distinct decisive-side patterns generate linear restrictions on the same unknown vector $\omega(x)$. Once $\omega(x)$ is identified at sufficiently many feature values, the affine structure of the gate recovers (α_f, β_f) rule by rule.

Theorem 1 (Fixed-feature identification of rule weights). *Fix $x \in \mathbb{R}^d$ and define*

$$\mathcal{A}_2(x) := \{A \in \mathcal{A}_2 : \psi(A) = x\}.$$

For each $A \in \mathcal{A}_2(x)$, let

$$h_f(A) := \kappa_f^L(A) - r(A)\kappa_f^R(A), \quad r(A) := \frac{p(A)}{1 - p(A)}.$$

Define the cellwise identified set

$$\Omega(x) := \left\{ \omega \in \mathbb{R}_{++}^{|\mathcal{F}|} : h(A)^\top \omega = 0 \quad \forall A \in \mathcal{A}_2(x) \right\}.$$

Assume $\Omega(x) \neq \emptyset$ (this is guaranteed under correct specification: the true weights $\omega_f(x) = \exp(\alpha_f + \beta_f^\top x)$ are strictly positive by construction, so $\omega(x) \in \Omega(x)$). Then the following are equivalent:

(i) $\Omega(x)$ is a single positive ray, i.e. there exists $\omega^*(x) \in \mathbb{R}_{++}^{|\mathcal{F}|}$ such that

$$\Omega(x) = \{c\omega^*(x) : c > 0\};$$

(ii) the row span of $\{h(A) : A \in \mathcal{A}_2(x)\}$ has dimension $|\mathcal{F}| - 1$.

Equivalently, if $H(x)$ is any stacked matrix whose rows span the same subspace as $\{h(A) : A \in \mathcal{A}_2(x)\}$, then

$$\Omega(x) \text{ is a single positive ray} \iff \text{rank } H(x) = |\mathcal{F}| - 1.$$

Under the normalization $\omega_{f_0}(x) = 1$, this is equivalent to point identification of $\omega(x)$.

Proof sketch. The model implies $h(A)^\top \omega(x) = 0$ for every $A \in \mathcal{A}_2(x)$, so $\Omega(x)$ is the set of strictly positive vectors in the null space of the stacked matrix $H(x)$. If $\text{rank } H(x) = |\mathcal{F}| - 1$, the null space is one-dimensional and $\Omega(x)$ is a single positive ray; the converse follows because, if the null space has dimension at least two and already contains one strictly positive vector (namely the true $\omega(x)$), then a sufficiently small perturbation along an independent null-space direction yields a second, non-proportional positive vector that still lies in the positive orthant. See Appendix B for the full proof. \square

The key identifying force in Theorem 1 is *rule switching at fixed features*: menus sharing the same $\psi(A) = x$ share the same latent weight vector $\omega(x)$, but may differ in which rules recommend which option. Each such menu contributes a linear restriction $h(A)^\top \omega(x) = 0$, and identification occurs when these restrictions span a codimension-one subspace of $\mathbb{R}^{|\mathcal{F}|}$.

From fixed-feature weights to global identification of the affine gate. Theorem 1 identifies the first-stage object $\omega(x)$ feature value by feature value. The next result shows that once these weight vectors are recovered at sufficiently many affinely independent feature values, the affine gate parameters themselves are globally identified.

Corollary 2 (Global identification from fixed-feature weights). *Consider the CA-RRM with affine indices*

$$s_f(A) = \alpha_f + \beta_f^\top \psi(A), \quad f \in \mathcal{F},$$

and impose the normalization

$$(\alpha_{f_0}, \beta_{f_0}) = (0, 0)$$

for some baseline rule $f_0 \in \mathcal{F}$. Let $d = \dim(\psi)$. Suppose there exist $(d + 1)$ feature values $x^{(0)}, \dots, x^{(d)}$ such that:

(G1) **Cellwise identification:** For each $k \in \{0, \dots, d\}$, there exist menus A_{k1}, \dots, A_{kM_k} with $\psi(A_{km}) = x^{(k)}$ for all m , such that the associated matrix

$$H^{(k)} := \begin{pmatrix} h(A_{k1})^\top \\ \vdots \\ h(A_{kM_k})^\top \end{pmatrix}$$

has rank $|\mathcal{F}| - 1$.

(G2) **Affine richness of feature values:** The matrix

$$X := \begin{pmatrix} 1 & (x^{(0)})^\top \\ \vdots & \vdots \\ 1 & (x^{(d)})^\top \end{pmatrix}$$

has full rank $d + 1$.

Then the full parameter vector $\{(\alpha_f, \beta_f)\}_{f \in \mathcal{F}}$ is globally identified from the population objects $\{p(A), \kappa^L(A), \kappa^R(A), \psi(A)\}$, up to the normalization.

Proof sketch. By Theorem 1, (G1) identifies each $\omega(x^{(k)})$ up to scale; the normalization $\omega_{f_0} \equiv 1$ pins the scale. For each rule f , stacking $\log \omega_f(x^{(k)}) = \alpha_f + \beta_f^\top x^{(k)}$ over $k = 0, \dots, d$ gives a linear system with coefficient matrix X , which is invertible by (G2). See Appendix C for the detailed version. \square

The corollary separates global identification into two conceptually distinct requirements. Condition (G1) is a within-feature condition: it uses rule switching across menus that share the same feature value to identify the relative rule weights at that feature value. Condition (G2) is an across-feature condition: it uses affine variation in the feature values themselves to map the identified weight vectors back into the gate coefficients. Thus, the identification argument has a clear two-step structure: first recover $\omega(x)$ locally in feature space, then recover the affine law of motion of those weights globally.

Effective dimension and baseline specification. Corollary 2 is stated for a generic feature map ψ . In our baseline specification (Section 6.6), the gate operates on a 12-dimensional vector of interpretable summary statistics $z(A) \in \mathbb{R}^{12}$, so the corollary applies with $\psi = z$. When this feature vector has structural redundancies (e.g., exact linear dependencies among coordinates), the corollary applies with d replaced by the effective dimension

$$d_{\text{eff}} := \text{rank}([\mathbf{1}, z]) - 1,$$

and identification holds for the gate parameters projected onto the effective feature subspace (i.e., up to the null space of $[\mathbf{1}, z]$). In our application, $d_{\text{eff}} = 11$ (the expected-value gap is a linear combination of the two level expected values). The neural benchmark models use a separate, higher-dimensional raw menu encoding $\psi(A) \in \mathbb{R}^{4M}$ as their input (Section 6.3); the identification conditions and diagnostics below do not target that encoding.

Diagnostics: empirically assessing identification strength

Theorem 1 and Corollary 2 reduce global identification to two verifiable ingredients on the observed support: cellwise rank sufficiency and affine richness of the identifying feature values. We report three diagnostics.

D1 (Two-sidedness). Report the fraction of menus that are two-sided:

$$\widehat{\Pr}(A \in \mathcal{A}_2).$$

This ensures that the log-odds representation (9) is empirically meaningful.

D2 (Coverage and side-variation by rule). For each rule f , report (i) decisiveness frequency $\widehat{\Pr}(A_f(A) = 1)$ and (ii) side-variation conditional on decisiveness:

$$\widehat{\Pr}(f \in \mathcal{I}_L(A) \mid A_f(A) = 1), \quad \widehat{\Pr}(f \in \mathcal{I}_R(A) \mid A_f(A) = 1).$$

Rules that take both sides contribute sign-varying rows to the $H^{(k)}$ matrices, supporting condition (G1).

D3 (Verification of (G1) and (G2)). The diagnostic is implemented on the interpretable gate features $z(A) \in \mathbb{R}^{12}$ used in the baseline specification (Section 6.6). To check (G1), group menus into cells that share the same (or nearby) value of $z(A)$, and compute $\text{rank}(H^{(k)})$ for each cell via singular value decomposition (SVD). Condition (G1) is supported if at least $d_{\text{eff}} + 1$ cells achieve $\text{rank } |\mathcal{F}| - 1$, where d_{eff} is the effective dimension of the gate feature space. Among the cells satisfying (G1), check that their representative feature values span $\mathbb{R}^{d_{\text{eff}}}$ affinely; (G2) is supported if this affine rank condition holds.

Checking (G1) in practice. Because the gate features $z(A)$ are 12-dimensional summary statistics, many distinct menus share the same (or very close) feature value. We group menus into cells \mathcal{C}_k using exact equality of $z(A)$ where possible, supplemented by k -means clustering as a finite-sample heuristic. We retain cells with at least $|\mathcal{F}| - 1$ menus. For each cell, we form the matrix

$$\hat{H}^{(k)}$$

by stacking the row vectors

$$\hat{h}(A)^\top = (\kappa_f^L(A) - \hat{r}(A)\kappa_f^R(A))_{f \in \mathcal{F}}$$

over its menus (trimming $\hat{p}(A)$ to $[\varepsilon, 1 - \varepsilon]$ for numerical stability), and compute its numerical rank via SVD.³ Assumption (G1) is supported if at least $d_{\text{eff}} + 1$ cells achieve

$$\text{rank}(\hat{H}^{(k)}) = |\mathcal{F}| - 1.$$

To verify (G2), we check that the centroids of cells satisfying (G1) are affinely independent.

If ψ is essentially injective (as with the raw 40-dimensional menu encoding), the sufficient global identification condition (G1) is not applicable, since no feature value is shared by multiple distinct menus. For completeness, Appendix O provides a local identification argument based on the Jacobian rank that does not require within-feature replication.

D1–D2 document that the model generates informative variation in left/right decisive sets. D3 provides empirical support for the sufficient conditions of Corollary 2 under the baseline gate specification with $z(A)$. We report the empirical results of these diagnostics on the Choices13k dataset in Section 7.1.

4 Rule library

The library described below is deliberately small and simple. Each element is a parameter-free heuristic that can be stated as a single line of conduct, implemented deterministically menu-by-menu, and produces a strict recommendation whenever it yields an unambiguous dominance comparison. Rather than postulating a global valuation model and fitting preference parameters, we treat behavior as switching among a few coarse procedures.

³With estimated $\hat{r}(A)$, the matrix $\hat{H}^{(k)}$ generically has full algebraic column rank $|\mathcal{F}|$ once the cell contains enough menus. We therefore check approximate rank deficiency by retaining singular values above a tolerance $\tau = 10^{-8} \times \sigma_1(\hat{H}^{(k)})$, where σ_1 is the largest singular value. (G1) is supported when the gap between $\sigma_{|\mathcal{F}|-1}$ and $\sigma_{|\mathcal{F}|}$ is large relative to τ , so that the rank- $(|\mathcal{F}| - 1)$ structure is robust to perturbations from sampling noise in $\hat{r}(A)$.

Notation. Let $\text{Supp}(L)$ be its finite support and let $x_{\min}(L) := \min \text{Supp}(L)$, $x_{\max}(L) := \max \text{Supp}(L)$. Write $\delta(z)$ for the degenerate lottery yielding z with probability one. Given outcomes $x, y \in \mathbb{R}$, define the (normalized) contrast

$$\text{contr}(x, y) := \frac{|x - y|}{|x| + |y| + 1}. \quad (12)$$

The outcomes x, y enter in their raw units (before the outcome rescaling applied to neural network features in Section 6.3). The constant $+1$ in the denominator is a fixed regularization choice (not a tunable parameter). Because the contrast is not homogeneous of degree zero, the effective rule recommendations depend on the outcome scale of the data. The rules remain parameter-free in the sense that no parameter is estimated from data, but they are not invariant to affine transformations of outcomes; applying the same rules to payoffs denominated in cents rather than dollars could change which rules are active on some menus. This scale dependence is a limitation of the current formulation. For some rules we use a small set of *extreme pairings*. For $A = \{L^1, L^2\}$ define

$$\mathcal{P}(A) := \{(a, b) : a \in \{x_{\min}(L^1), x_{\max}(L^1)\}, b \in \{x_{\min}(L^2), x_{\max}(L^2)\}\},$$

which contains at most four outcome pairs.⁴

Outcome simplification rules (MMn, MMA, MMx, MAP). These rules reduce each lottery to a single representative payoff (hence to a degenerate perceived lottery).

- MMN (security): “choose the option with the better worst-case outcome.”

$$\pi_{\text{MMN}}(L^i; L^j) := \delta(x_{\min}(L^i)).$$

- MMX (aspiration): “choose the option with the better best-case outcome.”

$$\pi_{\text{MMX}}(L^i; L^j) := \delta(x_{\max}(L^i)).$$

- MMA (midrange focus): “choose based on the midpoint between best and worst outcomes.”

$$\pi_{\text{MMA}}(L^i; L^j) := \delta\left(\frac{1}{2}(x_{\min}(L^i) + x_{\max}(L^i))\right).$$

- MAP (most-likely outcome): “choose the option whose most likely outcome is higher.” Let $z_{\text{mode}}(L)$ be the (highest) modal payoff of L (ties broken upward), then

$$\pi_{\text{MAP}}(L^i; L^j) := \delta(z_{\text{mode}}(L^i)).$$

⁴When $x_{\min}(L^i) = x_{\max}(L^i)$ for some lottery, $\mathcal{P}(A)$ may contain fewer than four distinct pairs. The notation $\{(a_k, b_k)\}_{k=1}^4$ should be understood as an indexed enumeration of the 2×2 grid (allowing repeats); the salience-score and ordering operations below remain well-defined in all cases.

Salience rules (SAL, SAL2). These rules formalize “attention to what stands out.” They compare the options using one salient extreme pairing. Let $\mathcal{P}(A) = \{(a_k, b_k)\}_{k=1}^4$ and define salience scores $c_k := \text{contr}(a_k, b_k)$.

- SAL (most salient comparison): “choose according to the single most salient extreme comparison.” Let $k^* \in \arg \max_k c_k$ (ties broken deterministically). Define

$$\pi_{\text{SAL}}(L^1; L^2) := \delta(a_{k^*}), \quad \pi_{\text{SAL}}(L^2; L^1) := \delta(b_{k^*}).$$

- SAL2 (second-most salient comparison): “choose according to the second most salient extreme comparison.” Let $c_{(1)} \geq c_{(2)}$ denote the two largest values among $\{c_k\}_{k=1}^4$ and let $k^{(2)}$ be an index attaining $c_{(2)}$. When $c_{(1)} = c_{(2)}$ the rule is left inactive (no well-defined “second” salient comparison); otherwise set

$$\pi_{\text{SAL2}}(L^1; L^2) := \delta(a_{k^{(2)}}), \quad \pi_{\text{SAL2}}(L^2; L^1) := \delta(b_{k^{(2)}}).$$

Regret rules (REG, REGmed). Following Loomes and Sugden (1982), these rules define the state space as the set of all outcome pairs (x_i, y_j) with $x_i \in \text{Supp}(L^1)$, $y_j \in \text{Supp}(L^2)$, each occurring with probability $p_i^{L^1} \cdot p_j^{L^2}$. In state (i, j) , the regret of choosing L^1 is $d_{ij}^L := [y_j - x_i]_+$ and the regret of choosing L^2 is $d_{ij}^R := [x_i - y_j]_+$.

- REG (regret-distribution dominance): “choose the option whose negated-regret distribution first-order stochastically dominates.” The perceived lottery for L^1 given L^2 is the full negated-regret distribution (i.e., the distribution of $-d_{ij}^L$, so that “larger is better” under the usual FSD convention)

$$\pi_{\text{REG}}(L^1; L^2) := \sum_{i,j} p_i^{L^1} p_j^{L^2} \delta(-d_{ij}^L), \quad \pi_{\text{REG}}(L^2; L^1) := \sum_{i,j} p_i^{L^1} p_j^{L^2} \delta(-d_{ij}^R).$$

The rule is active when one negated-regret distribution strictly first-order stochastically dominates the other.

- REGMED (median regret): “choose the option with the smaller probability-weighted median regret.”

$$R_{\text{med}}^L := \text{wmed}(\{d_{ij}^L\}, \{p_i^{L^1} p_j^{L^2}\}), \quad R_{\text{med}}^R := \text{wmed}(\{d_{ij}^R\}, \{p_i^{L^1} p_j^{L^2}\}),$$

where wmed denotes the weighted median; then $\pi_{\text{REGMED}}(L^1; L^2) := \delta(-R_{\text{med}}^L)$ and $\pi_{\text{REGMED}}(L^2; L^1) := \delta(-R_{\text{med}}^R)$.

Disappointment rules (DIS, DISmed). These rules treat the most likely outcome as a reference point and penalize downside contrasts below it. For a lottery L , let $z_{\text{mode}}(L)$ be its (highest) modal payoff, and define the set of downside payoffs $Z^-(L) := \{z \in \text{Supp}(L) : z < z_{\text{mode}}(L)\}$. Define the disappointment contrasts $s(z) := \text{contr}(z_{\text{mode}}(L), z)$ for $z \in Z^-(L)$ (and set the index to 0 if $Z^-(L) = \emptyset$).

- DIS (worst-case disappointment): “avoid the option with the largest downside contrast below its most likely outcome.”

$$D(L) := \max_{z \in Z^-(L)} s(z) \quad (\text{with } D(L) = 0 \text{ if } Z^-(L) = \emptyset), \quad \pi_{\text{DIS}}(L^i; L^j) := \delta(-D(L^i)).$$

- DISMED (typical downside disappointment): “avoid the option with the second-largest downside contrast below its most likely outcome.” If $|Z^-(L)| \geq 2$, let $s_{(1)} \geq s_{(2)} \geq \dots$ be the sorted contrasts and set $D_{\text{med}}(L) := s_{(2)}$; otherwise set $D_{\text{med}}(L) := D(L)$. Then

$$\pi_{\text{DISMED}}(L^i; L^j) := \delta(-D_{\text{med}}(L^i)).$$

Extreme attention rules (A1, A2). The last group encodes extreme one-sided consideration sets. Fix $M > 0$ so that $-M$ lies strictly below all payoffs in the dataset.

- A1 (attention to L^1): “treat the right option as an extremely bad sure outcome.”

$$\pi_{\text{A1}}(L^1; L^2) = L^1, \quad \pi_{\text{A1}}(L^2; L^1) = \delta(-M).$$

- A2 (attention to L^2): symmetric.

$$\pi_{\text{A2}}(L^1; L^2) = \delta(-M), \quad \pi_{\text{A2}}(L^2; L^1) = L^2.$$

In our implementation, both A1 and A2 are always included; they also ensure that at least one rule is decisive at essentially every menu, which stabilizes the CA-RRM normalization in (3).

Discussion

The library spans five broad mechanisms emphasized in behavioral and bounded-rationality work—outcome simplification, salience-driven attention, regret, disappointment, and limited consideration—implemented here in a deliberately coarse, parameter-free form. The gate does not estimate a valuation model; it learns when each simple line of conduct best predicts behavior.

Within-family variants and why we avoid “aggregate” rules. Several rules are variants within a common mechanism (e.g. SAL vs. SAL2, REG vs. REGMED). When two variants are active at the same menu, the conditional-on-activity weights (5) yield a direct within-family split. A natural alternative would be a single “aggregate” rule that combines information across all ranks, but such a rule requires specifying how ranks are weighted—absent preference parameters there is no canonical choice. We instead use discrete variants (top-ranked vs. second-ranked comparison) that probe sensitivity to the ranking without introducing an explicit aggregation scheme, stopping at rank two to keep the library small.

4.1 Rule-level Diagnostics

The rule-gating predictor is transparent at the menu level: by (6), each predicted choice probability is a convex combination of deterministic rule recommendations, with weights $\tilde{q}_f(A; \hat{\theta})$ that can be interpreted as *conditional-on-activity responsibilities*. This section introduces summary diagnostics that turn these menu-by-menu decompositions into interpretable rule-level statements. The goal is twofold: (i) quantify which procedures the fitted gate actually uses on average, and (ii) distinguish rules that are essential for fit from rules that mainly act as substitutes.

Effective responsibility weights and concentration

Because the CA-RRM conditions on activity, the economically meaningful notion of “rule usage” is the gate mass *among decisive rules*. For each menu A_t and each rule f , define the effective responsibility

$$\tilde{q}_{tf} := \tilde{q}_f(A_t; \hat{\theta}) = \frac{q_f(A_t; \hat{\theta}) A_f(A_t)}{\sum_{g \in \mathcal{F}} q_g(A_t; \hat{\theta}) A_g(A_t)}, \quad (13)$$

whenever the denominator is positive.⁵ The *effective responsibility weight* of rule f is the average responsibility across menus,

$$w_f := \frac{1}{T} \sum_{t=1}^T \tilde{q}_{tf}, \quad \sum_{f \in \mathcal{F}} w_f = 1. \quad (14)$$

Thus w_f measures the average share of decision mass attributed to rule f , *conditional on the rule being eligible to speak* (i.e., active) at each menu.

Rule Concentration

To summarize whether the fitted mixture concentrates on a few procedures or is diffuse across many, we report the Herfindahl concentration of responsibility weights,

$$\text{HHI}(F) := \sum_{f \in \mathcal{F}} w_f^2. \quad (15)$$

Higher $\text{HHI}(F)$ indicates that a small subset of rules accounts for most effective responsibility, whereas lower $\text{HHI}(F)$ indicates a more even allocation across rules. This statistic is informative because the rule-gating predictor is interpretable only to the extent that its effective responsibilities are *parsimonious*: a high concentration means that most menus are explained by a small repertoire of named procedures, while a low concentration suggests that predictive success relies on a broad set of substitutes. We also report the *effective number of rules*

$$N_{\text{eff}}(F) := \frac{1}{\text{HHI}(F)} \in [1, |\mathcal{F}|],$$

which can be read as the number of equally-weighted rules that would generate the same concentration. For example, $N_{\text{eff}} = 3$ means that the fitted model is about as concentrated as one that splits effective responsibility evenly across three procedures. We use $\text{HHI}(F)$ (and N_{eff}) as a compact summary of whether the fitted rule-gating model achieves accuracy through a few unifying mechanisms or through a diffuse patchwork of rules.

Predictive ablation index $\phi(f)$

Responsibility weights are descriptive, but they do not by themselves tell whether a rule is *necessary* for predictive accuracy: a rule can carry substantial mass yet be redundant because other rules typically make the same recommendation, and conversely a rarely-used rule can matter sharply in

⁵In our implementation, the two attention rules A1 and A2 are always included and are decisive for essentially all menus, so the denominator is typically well away from zero.

a small region of menu space. To quantify importance for fit, we use a refit-and-compare ablation diagnostic.

For each rule $f \in \mathcal{F} \setminus \{A1, A2\}$, let MSE^{-f} denote the cross-validated test MSE of rule-gating when f is removed from the library and the gate is retrained on the remaining rules. Let MSE^{full} be the corresponding MSE for the full library. Define

$$\phi(f) := \frac{\text{MSE}^{-f} - \text{MSE}^{\text{full}}}{\text{MSE}^{\text{full}}}. \quad (16)$$

Thus $\phi(f) > 0$ means that removing f worsens out-of-sample accuracy, and larger values indicate a more prediction-critical procedure.⁶

Concentration impact $\sigma_N(f)$

Finally, we ask whether a rule acts as a *unifier* (its presence makes effective responsibility concentrate on a small repertoire of procedures) or instead as a *substitute* that helps spread responsibility across the library. For each $f \in \mathcal{F} \setminus \{A1, A2\}$, we refit the gate after removing f and recompute the effective responsibility weights and concentration. Let HHI^{-f} denote the resulting concentration, and let $N_{\text{eff}}^{-f} := 1/\text{HHI}^{-f}$ be the associated effective number of rules (recall $N_{\text{eff}}(F) = 1/\text{HHI}(F)$ from above). We summarize the *concentration impact* of rule f by the relative change in the effective number of rules:

$$\sigma_N(f) := \frac{N_{\text{eff}}^{-f} - N_{\text{eff}}(F)}{N_{\text{eff}}(F)}. \quad (17)$$

Thus $\sigma_N(f) > 0$ means that removing f increases the effective number of rules (the fitted mixture becomes more diffuse). Conversely, $\sigma_N(f) < 0$ means that removing f decreases the effective number of rules (the mixture becomes more concentrated), so f primarily acts as a substitute/diversifier: when it is unavailable, the gate reallocates mass more sharply onto a smaller set of remaining procedures. This refit-based diagnostic complements the ablation index $\phi(f)$: $\phi(f)$ measures the *predictive* importance of f , while $\sigma_N(f)$ measures its role in shaping the *structure* of the fitted mixture. Importantly, $\sigma_N(f)$ is computed after a full refit and therefore reflects equilibrium reallocation of responsibility.

The pair $(\phi(f), \sigma_N(f))$ separates distinct roles. A large $\phi(f)$ indicates that the procedure improves predictive fit and is not easily replaced by the rest of the library; the sign and magnitude of $\sigma_N(f)$ indicate whether that procedure also shapes the overall mixture structure (concentrating or diversifying effective responsibility). In Section 7 we report $(w_f, \phi(f), \sigma_N(f))$ side-by-side to identify rules that are heavily used, rules that are essential for accuracy, and rules that mainly act as substitutes or robustness variants.

5 Estimation and inference

The identification results suggest a constructive two-step estimator. The first step recovers, at feature values satisfying the fixed-feature rank condition, the vector of relative rule weights. The second step uses the affine restriction on log-weights to recover the gate parameters. This section

⁶We exclude A1/A2 from ablation because they serve as stability anchors by ensuring decisiveness at essentially every menu; dropping them would confound behavioral importance with numerical degeneracy of the CA-RRM normalization.

treats the econometric object of interest—latent procedural heterogeneity—separately from the gradient-based prediction procedure used later for model comparison.

Sampling scheme. Let $\mathcal{M} = \{A_1, \dots, A_M\}$ be a finite collection of menus. For each menu A_m , we observe n_m independent binary choices $Y_{mi} \in \{0, 1\}$, $i = 1, \dots, n_m$, with

$$\Pr(Y_{mi} = 1 \mid A_m) = p(A_m) \in (0, 1).$$

For distinct menus, the menu-specific samples are mutually independent. Write

$$\hat{p}_m := \frac{1}{n_m} \sum_{i=1}^{n_m} Y_{mi}, \quad \hat{r}_m := \frac{\hat{p}_m}{1 - \hat{p}_m},$$

where, for numerical stability only, \hat{p}_m may be trimmed to $[\varepsilon_n, 1 - \varepsilon_n]$ with $\varepsilon_n \downarrow 0$ slowly enough that trimming is asymptotically inactive.

We study the asymptotic regime

$$N := \min_{1 \leq m \leq M} n_m \rightarrow \infty, \quad \frac{n_m}{N} \rightarrow \pi_m \in (0, \infty) \quad \text{for each } m.$$

Identifying feature values. Let $x^{(1)}, \dots, x^{(K)}$ be distinct feature values with $K \geq d + 1$, and define the associated menu cells

$$\mathcal{M}_k := \{m \in \{1, \dots, M\} : \psi(A_m) = x^{(k)}\}.$$

For each k , let $M_k := |\mathcal{M}_k|$ and assume $M_k \geq |\mathcal{F}| - 1$. For $m \in \mathcal{M}_k$, define

$$h_f(A_m) := \kappa_f^L(A_m) - r(A_m)\kappa_f^R(A_m), \quad \hat{h}_f(A_m) := \kappa_f^L(A_m) - \hat{r}_m \kappa_f^R(A_m).$$

Let $H^{(k)}$ and $\hat{H}^{(k)}$ denote the $M_k \times |\mathcal{F}|$ matrices stacking the row vectors $h(A_m)^\top$ and $\hat{h}(A_m)^\top$ over $m \in \mathcal{M}_k$.

Fix the baseline rule f_0 , and reorder coordinates so that f_0 is first. Partition

$$H^{(k)} = [h_0^{(k)} \quad H_-^{(k)}], \quad \hat{H}^{(k)} = [\hat{h}_0^{(k)} \quad \hat{H}_-^{(k)}],$$

where $h_0^{(k)}$ is the first column and $H_-^{(k)}$ collects the remaining $|\mathcal{F}| - 1$ columns.

First-stage estimator: cellwise rule weights. Under Theorem 1, the normalized weight vector at $x^{(k)}$ is uniquely determined by $\omega_{f_0}(x^{(k)}) = 1$ and

$$H^{(k)}\omega(x^{(k)}) = 0.$$

Writing

$$\omega(x^{(k)}) = (1, \eta^{(k)\top})^\top, \quad \eta^{(k)} \in \mathbb{R}^{|\mathcal{F}|-1},$$

the population vector $\eta^{(k)}$ solves

$$H_-^{(k)}\eta^{(k)} = -h_0^{(k)}.$$

When $\text{rank } H^{(k)} = |\mathcal{F}| - 1$, this system has the unique least-squares solution

$$\eta^{(k)} = -\left(H_-^{(k)\top} H_-^{(k)}\right)^{-1} H_-^{(k)\top} h_0^{(k)}.$$

We therefore define the sample estimator

$$\hat{\eta}^{(k)} := -\left(\hat{H}_-^{(k)\top} \hat{H}_-^{(k)}\right)^{-1} \hat{H}_-^{(k)\top} \hat{h}_0^{(k)}, \quad \hat{\omega}(x^{(k)}) := (1, \hat{\eta}^{(k)\top})^\top. \quad (18)$$

Because the true normalized weight vector is strictly positive, positivity of $\hat{\omega}(x^{(k)})$ holds with probability approaching one.

Second-stage estimator: affine gate parameters. For each non-baseline rule $f \neq f_0$, define

$$\gamma_f := (\alpha_f, \beta_f^\top)^\top \in \mathbb{R}^{d+1}, \quad z_k := (1, x^{(k)\top})^\top.$$

The affine gate implies

$$\log \omega_f(x^{(k)}) = z_k^\top \gamma_f, \quad k = 1, \dots, K.$$

Hence, once the first-stage weights are estimated, the second stage is a linear regression of estimated log-weights on the identifying feature values:

$$\hat{y}_f^{(k)} := \log \hat{\omega}_f(x^{(k)}).$$

Let

$$X_K := \begin{pmatrix} z_1^\top \\ \vdots \\ z_K^\top \end{pmatrix}.$$

For any positive definite weight matrix $W_f \in \mathbb{R}^{K \times K}$, define the minimum-distance estimator

$$\hat{\gamma}_f := \arg \min_{\gamma \in \mathbb{R}^{d+1}} (\hat{y}_f - X_K \gamma)^\top W_f (\hat{y}_f - X_K \gamma) = (X_K^\top W_f X_K)^{-1} X_K^\top W_f \hat{y}_f. \quad (19)$$

When $K = d + 1$, this collapses to exact inversion:

$$\hat{\gamma}_f = X_K^{-1} \hat{y}_f.$$

Population functionals. The two-step estimator identifies the economically meaningful functionals of the gate. On the menu support \mathcal{M} , examples include:

$$\begin{aligned} \bar{q}_f(\theta) &:= \frac{1}{M} \sum_{m=1}^M q_f(A_m; \theta), \\ \bar{a}_f(\theta) &:= \frac{1}{M} \sum_{m=1}^M q_f(A_m; \theta) A_f(A_m), \\ w_f(\theta) &:= \frac{1}{M} \sum_{m=1}^M \frac{q_f(A_m; \theta) A_f(A_m)}{\sum_{g \in \mathcal{F}} q_g(A_m; \theta) A_g(A_m)}. \end{aligned}$$

These correspond, respectively, to average latent gate mass, average effective active mass, and average conditional-on-activity responsibility.

Assumption 1. The following hold:

- (E1) **Interior probabilities.** There exists $\underline{p} \in (0, 1/2)$ such that $p(A_m) \in [\underline{p}, 1 - \underline{p}]$ for all m .
- (E2) **Cellwise identification.** For each $k = 1, \dots, K$, the matrix $H^{(k)}$ has rank $|\mathcal{F}| - 1$.
- (E3) **Affine richness.** The matrix X_K has full column rank $d + 1$.
- (E4) **Interior weights.** For every k and every $f \neq f_0$, $\omega_f(x^{(k)}) \geq \underline{\omega}$ for some $\underline{\omega} > 0$.
- (E5) **Stable sampling shares.** $n_m/N \rightarrow \pi_m \in (0, \infty)$ for each menu m .

Theorem 3 (Consistency and asymptotic normality of the two-step estimator). *Under Assumption 1:*

(i) For each $k = 1, \dots, K$,

$$\hat{\omega}(x^{(k)}) \xrightarrow{p} \omega(x^{(k)}), \quad \sqrt{N} \left(\hat{\omega}(x^{(k)}) - \omega(x^{(k)}) \right) \xrightarrow{d} \mathcal{N}(0, V_\omega^{(k)}).$$

In particular, applying the log transformation under (E4),

$$\sqrt{N} \left(\hat{y}_f^{(k)} - \log \omega_f(x^{(k)}) \right) \xrightarrow{d} \mathcal{N}(0, V_{y,f}^{(k)}) \quad \text{for each } f \neq f_0.$$

Stacking across cells, $\sqrt{N}(\hat{y}_f - y_f) \xrightarrow{d} \mathcal{N}(0, V_{y,f})$ where $\hat{y}_f := (\hat{y}_f^{(1)}, \dots, \hat{y}_f^{(K)})^\top$ and $V_{y,f} = \text{diag}(V_{y,f}^{(1)}, \dots, V_{y,f}^{(K)})$.

(ii) For each non-baseline rule $f \neq f_0$,

$$\hat{\gamma}_f \xrightarrow{p} \gamma_f, \quad \sqrt{N}(\hat{\gamma}_f - \gamma_f) \xrightarrow{d} \mathcal{N}(0, V_{\gamma,f}),$$

where

$$V_{\gamma,f} = (X_K^\top W_f X_K)^{-1} X_K^\top W_f V_{y,f} W_f X_K (X_K^\top W_f X_K)^{-1}.$$

(iii) For any functional $\tau(\theta)$ that is continuously differentiable at the true parameter vector,

$$\hat{\tau} := \tau(\hat{\theta})$$

is consistent and satisfies

$$\sqrt{N}(\hat{\tau} - \tau(\theta_0)) \xrightarrow{d} \mathcal{N}(0, \nabla \tau(\theta_0)^\top V_\theta \nabla \tau(\theta_0)),$$

where V_θ is the asymptotic covariance matrix of the stacked estimator $\hat{\theta} = \{\hat{\gamma}_f\}_{f \neq f_0}$.

Proof sketch. For each menu m , the sample share \hat{p}_m is a sample mean of i.i.d. Bernoulli variables, so

$$\sqrt{n_m}(\hat{p}_m - p(A_m)) \xrightarrow{d} \mathcal{N}(0, p(A_m)(1 - p(A_m))).$$

Because $r(p) = p/(1 - p)$ is continuously differentiable on $[\underline{p}, 1 - \underline{p}]$, the delta method gives

$$\sqrt{n_m}(\hat{r}_m - r(A_m)) \xrightarrow{d} \mathcal{N}(0, \sigma_{r,m}^2).$$

Hence each $\hat{H}^{(k)}$ is a smooth perturbation of $H^{(k)}$. Under (E2), $H_-^{(k)\top} H_-^{(k)}$ is nonsingular, so the map

$$H^{(k)} \mapsto \eta^{(k)} = -(H_-^{(k)\top} H_-^{(k)})^{-1} H_-^{(k)\top} h_0^{(k)}$$

is continuously differentiable in a neighborhood of the truth. A second delta-method step yields consistency and asymptotic normality of $\hat{\eta}^{(k)}$, hence of $\hat{\omega}(x^{(k)})$ and $\hat{y}_f^{(k)}$. The second-stage estimator (19) is a linear map of \hat{y}_f , so its asymptotic properties follow immediately. The final statement is a standard delta-method consequence. The full proof is given in Appendix D. \square

Efficient weighting and feasible inference. A natural choice is feasible GLS, using a consistent estimator $\hat{V}_{y,f}$ of the first-stage covariance matrix and setting $W_f = \hat{V}_{y,f}^{-1}$. In practice, because the covariance formulas inherit the first-stage delta-method Jacobian, a cluster bootstrap at the menu level is attractive and directly yields standard errors for both the affine coefficients and the decomposition functionals \bar{q}_f , \bar{a}_f , and w_f .

Overidentification test of the affine gate. When $K > d + 1$, the affine gate restriction is overidentified. For each rule $f \neq f_0$, define the second-stage residual vector

$$\hat{u}_f := \hat{y}_f - X_K \hat{\gamma}_f.$$

A natural minimum-distance specification test is

$$J_f := N \hat{u}_f^\top \hat{V}_{y,f}^{-1} \hat{u}_f,$$

where $\hat{V}_{y,f}$ is a consistent estimator of $V_{y,f}$ (the asymptotic variance of $\sqrt{N}(\hat{y}_f - y_f)$ from Theorem 3). Under efficient weighting ($W_f = V_{y,f}^{-1}$) and the null that $\log \omega_f(x)$ is affine in x , standard minimum-distance theory gives the asymptotic reference distribution $J_f \xrightarrow{d} \chi_{K-d-1}^2$. A joint test across rules can be formed analogously by stacking the residuals.

The two-step estimator targets identification-consistent parameter recovery and supports inference on economically meaningful functionals. For out-of-sample prediction and model comparison, we rely on the MSE-based predictive estimator described in Section 6.5.

6 Data and empirical design

This section introduces the data and evaluation protocol. We describe the dataset, define the prediction target and evaluation metric, explain the gate-feature specification on which the identification conditions of Section 3 are verified, and detail the cross-validation protocol used for predictive comparison. Benchmark models are described at the end of the section.

6.1 Dataset and target variable

We use the `choices13k` dataset introduced by Peterson et al. (2021), containing 13,006 binary risky-choice problems. Each problem corresponds to a menu $A = \{L^1, L^2\}$ and is repeated across many observations, allowing the computation of a menu-level choice frequency. We work with the filtered dataset that (i) removes ambiguous problems (masked probabilities) and (ii) keeps only problems for which feedback was provided, yielding $T = 9,831$ menus. The feedback restriction

follows the baseline protocol of Peterson et al. (2021) and has a practical justification: feedback problems have more repetitions per menu, producing more precise estimates of the choice frequency $\hat{p}(A)$ that serves as our prediction target. Because our model is static (it maps menu features to a predicted choice probability without using feedback information), the feedback condition affects only the precision of the dependent variable, not the model’s information set.⁷ For each menu A , the dataset reports the fraction of times the left option is chosen. We denote this empirical frequency by $\hat{p}(A)$ and treat it as the target to be predicted.

6.2 Evaluation metric

Our main performance metric is the mean squared error (MSE):

$$\text{MSE}(g) = \frac{1}{T} \sum_{t=1}^T \left(g(A_t) - \hat{p}(A_t) \right)^2, \quad (20)$$

for $\{A_t\}_{t \in \{1, \dots, T\}} \subseteq \mathcal{A}_{\text{full}}$. The MSE is a scoring rule: it rewards probabilistic accuracy and penalizes both systematic bias and overconfidence. We focus on MSE because it is standard and is the primary metric reported by Peterson et al. (2021).

Because the number of trials $n(A_t)$ behind each menu-level frequency $\hat{p}(A_t)$ varies across menus, we also report a trial-weighted variant:

$$\text{MSE}_w(g) = \frac{\sum_{t=1}^T n(A_t) \left(g(A_t) - \hat{p}(A_t) \right)^2}{\sum_{t=1}^T n(A_t)}. \quad (21)$$

This metric downweights menus estimated from few trials, where $\hat{p}(A_t)$ is noisier, and gives a more precision-aware summary of predictive accuracy. We use the unweighted MSE as the primary metric for comparability with Peterson et al. (2021) and report MSE_w as a robustness check.

We also conduct paired split-level comparisons: for each pair of models, we compute per-fold metric differences and report their mean and standard error across the 50 splits (Appendix Table A.2).

Target variable as estimate. The menu-level choice frequency $\hat{p}(A)$ is itself an estimate of $p(A)$, computed from a finite number of trials $n(A)$. We treat $\hat{p}(A)$ as the prediction target without modeling the sampling process. This is appropriate because Choices13k menus typically aggregate many repetitions (median above 25). The trial-weighted metric MSE_w provides a precision-aware robustness check, and rankings are preserved (Table 3). The fold-level variability bands measure instability from random train/test partitions (the design component), not sampling variability in the choice frequencies; the design component dominates in our setting.

6.3 Menu encoding

All models take as input a fixed-length numerical encoding of the two lotteries in the menu. To align with Peterson et al. (2021), each lottery is represented by its list of outcomes and probabilities

⁷Feedback can in principle induce learning effects. If such dynamics are present, our static model captures the average behavior under the feedback regime.

after sorting outcomes in increasing order, truncating to a maximum support size M and padding with zeros. We set $M = 10$ throughout.

Formally, for each lottery L with support points $\{(x_k, \pi_k)\}_{k=1}^K$, order outcomes so that $x_1 \leq \dots \leq x_K$ and define

$$x_{1:M}(L) = (x_1, \dots, x_{\min\{K, M\}}, 0, \dots, 0), \quad \pi_{1:M}(L) = (\pi_1, \dots, \pi_{\min\{K, M\}}, 0, \dots, 0).$$

The menu encoding is the concatenation

$$\psi(A) = \left(x_{1:M}(L^1), \pi_{1:M}(L^1), x_{1:M}(L^2), \pi_{1:M}(L^2) \right) \in \mathbb{R}^{4M}. \quad (22)$$

To stabilize optimization across models, we rescale outcomes by the maximum absolute payoff observed in the filtered sample; the same scaling is applied for all models and all folds. This rescaling enters only the menu encoding $\psi(A)$ (and hence the gate features $z(A)$) used as inputs to differentiable models; it does not affect the rule indicators, which are computed on raw outcomes before any rescaling. The scaling is a fixed, data-wide preprocessing step applied identically to all models and folds.

6.4 Cross-validation protocol

We compare models using the out-of-sample evaluation structure of Peterson et al. (2021). The unit of observation for prediction is the menu, not the individual trial. We repeatedly split the set of menus into training and test sets, fit model parameters on the training set, and evaluate MSE on the held-out test set.

Splits. We generate $K = 50$ independent random splits of the N menus into 90% training and 10% test, as in Peterson et al. (2021). Each model is trained from scratch on each split.

Learning-rate selection. Each differentiable model is trained by gradient descent (Adam). Following Peterson et al. (2021), we select the learning rate from a small grid. To avoid selecting the learning rate on the same data used to evaluate generalization (as in Peterson et al., 2021, who select on test MSE), we use a two-pass protocol within each split. In Pass A (validation), we further partition the training set into an 80% sub-training set and a 20% validation set, train the model on the sub-training set for each candidate learning rate, and record the validation MSE. In Pass B (test), we retrain the model on the *full* training set using each candidate learning rate and evaluate MSE on the held-out test set. The reported performance of a model is the average test MSE (from Pass B) across the 50 splits at the learning rate that achieves the lowest average validation MSE (from Pass A). This two-pass validation protocol applies to all models *except* the Mixture of Theories (MOT). MOT relies on the HURD library’s internal training/validation logic, which does not expose hooks for overriding the train/validation partition or for extracting per-menu predictions at the validation stage. We therefore select MOT’s learning rate by mean *test* MSE across splits, following Peterson et al. (2021). This asymmetry is conservative: it gives MOT the benefit of test-set-informed learning-rate selection, which, if anything, biases the comparison in MOT’s favor.

Implementation details. We adopt the same network sizes and training horizons used by Peterson et al. (2021) (and their Supplementary Materials) for Neural EU/PT/CPT, Value-Based, Context-Dependent, and MOT. We keep all such hyperparameters fixed across splits and do not tune architectures. The only tuned hyperparameter is the learning rate.

6.5 Predictive implementation

For the purpose of out-of-sample prediction and model comparison, we estimate the gate parameters by direct MSE minimization. This predictive estimator differs from the two-step econometric procedure of Section 5: the latter targets the identification-driven parameter recovery and supports inference for rule-level functionals, while the former is designed purely for predictive accuracy and benchmark evaluation. The rule-gating model differs from the benchmark neural predictors in a key way: the *rules are deterministic and parameter-free*. Estimation concerns only the *gate*, i.e. the mapping from menu features $z(A)$ to rule propensities $q(A) \in \Delta^{F-1}$ (see Section 6.6 for the definition of $z(A)$).

Precomputation: rule activity and recommendations. For each menu A_t and each rule $f \in \mathcal{F}$, we compute once-and-for-all the indicators $A_f(A_t)$ and $L_f(A_t)$ defined in (1)–(2). These are deterministic functions of (A_t, f) . Precomputing them is important: it makes training fast and ensures that the gate is the only learned component.

Gate estimation. On a given training split, we estimate the gate parameters θ by minimizing the training MSE between the predicted choice probability $g_{\text{RG}}(A; \theta)$ and the target $\hat{p}(A)$, where

$$g_{\text{RG}}(A; \theta) = \frac{\sum_{f \in \mathcal{F}} q_f(A; \theta) L_f(A)}{\max\{\sum_{f \in \mathcal{F}} q_f(A; \theta) A_f(A), m_{\min}\}}.$$

The gate weights $q_f(A; \theta)$ are given by the softmax specification (4). We optimize the smooth objective using Adam with gradient clipping. This training step is conceptually simple: it is standard least-squares fitting, except that predictions are constructed as a weighted average of deterministic rule recommendations, conditional on rule activity.

6.6 Gate features

The gate’s role is to modulate rule responsibilities using observable features of the menu. A natural question is which features to use. We adopt as the baseline specification a 12-dimensional vector of economically motivated summary statistics $z(A) \in \mathbb{R}^{12}$. Six are *pairwise gaps* between the two lotteries: the expected-value gap $\text{EV}(L^1) - \text{EV}(L^2)$, the best-case outcome gap $\max(L^1) - \max(L^2)$, the worst-case outcome gap $\min(L^1) - \min(L^2)$, the variance gap $\text{Var}(L^1) - \text{Var}(L^2)$, the modal-outcome gap $\text{Mode}(L^1) - \text{Mode}(L^2)$, and the skewness gap $\text{Skew}(L^1) - \text{Skew}(L^2)$. These gaps are designed to capture the contrasts that the rules in the library operate on: the min/max gaps relate to MMN/MMX, the mode gap relates to MAP, and the EV and variance gaps relate to risk-return tradeoffs. The remaining six are *per-lottery or menu-level features*: the expected values $\text{EV}(L^1)$ and $\text{EV}(L^2)$, the standard deviations $\text{SD}(L^1)$ and $\text{SD}(L^2)$, the largest absolute outcome across both lotteries $\max_{i \in \{1,2\}} \max |\text{Supp}(L^i)|$, and the support-size gap $|\text{Supp}(L^1)| - |\text{Supp}(L^2)|$ (itself a pairwise difference, but included in this group because it measures menu complexity rather than

a preference-relevant contrast). These features allow the gate to condition rule propensities on the scale and complexity of the menu environment. By construction, $d_z = 12$ is much smaller than the $4M = 40$ dimensions of the raw encoding, but it captures the economically relevant variation: each feature has a direct verbal interpretation as a lottery comparison or a menu characteristic.

Why coarsen the gate input. Using a coarsened feature vector $z(A)$ rather than the raw menu encoding $\psi(A)$ is conceptually appropriate for the gate’s role. The gate is meant to capture systematic variation in rule usage with broad menu characteristics - scale, risk, tails, complexity - not to index menus individually. Coarsening yields repeated support points: many distinct menus share the same (or nearby) feature value $z(A)$, which is needed for the global identification conditions (G1)-(G2) to be empirically meaningful. With the raw 40-dimensional encoding, the mapping $A \mapsto \psi(A)$ is essentially injective, so the sufficient within-feature variation required by (G1) cannot literally occur. Finally, $z(A)$ is interpretable and portable across datasets, and in our application it matches or improves predictive accuracy relative to the raw encoding (Appendix N).

The gate uses the softmax architecture of Equation (4) with $z(A)$ in place of $\psi(A)$, giving $(|\mathcal{F}| - 1) \times (1 + d_z)$ free parameters. All neural benchmark models (Neural EU/PT/CPT, Value-Based, Context-Dependent, MOT) continue to use the raw encoding $\psi(A)$ as input, since they do not have a gate structure and the identification conditions do not apply to their parameterizations.

6.7 Benchmark models

We benchmark rule-gating against the main differentiable model classes studied by Peterson et al. (2021). For most benchmark classes, a model first assigns each gamble a value $V(\cdot)$ and then maps values into a choice probability via a logit (softmax) link:

$$g(A; \theta) = \frac{\exp(\eta V(L^1))}{\exp(\eta V(L^1)) + \exp(\eta V(L^2))}, \quad (23)$$

where η is a free “determinism” (inverse-noise) parameter. The exception is the fully context-dependent network, which directly outputs $g(A; \theta)$.

Neural EU. This class retains the expected-utility structure $V(L) = \sum_k p_k u(x_k)$ but learns the utility function $u(\cdot)$ as a small neural network, jointly with η .

Neural PT. This class retains the prospect-theory structure $V(L) = \sum_k u(x_k) \pi(p_k)$ but learns both $u(\cdot)$ and $\pi(\cdot)$ as neural networks, jointly with η .

Neural CPT. This class implements cumulative prospect theory with separate probability-weighting functions for gains and losses, applied cumulatively to ordered outcomes. The functions $u(\cdot)$ and $\pi^+(\cdot), \pi^-(\cdot)$ are learned by neural networks, jointly with η .

Value-Based. This class relaxes the linear aggregation of outcomes and probabilities within each gamble while still valuing gambles independently:

$$V(L) = f(x^L, p^L),$$

where f is a neural network taking the padded outcome and probability vectors as input; choice probabilities follow (23).

Context-Dependent. This is the most flexible differentiable benchmark: a neural network directly maps the full description of both gambles to a choice probability,

$$g(A; \theta) = f_{\text{NN}}(x^{L^1}, p^{L^1}, x^{L^2}, p^{L^2}),$$

without imposing a representation in terms of separate values $V(L^1), V(L^2)$.

Mixture of Theories (MOT). MOT is a structured context-dependent benchmark in which the model selects (softly) among a small set of subjective utility functions and probability-weighting functions using gating networks (a mixture-of-experts architecture) (Peterson et al., 2021, Supplementary Materials). Separate softmax gates output mixture weights for utilities and for probability weighting; values are computed by mixing two candidate utility functions and two candidate probability-weighting functions, and then mapped into a choice probability via (23). A separate component handles dominated gambles via an additional parameter (a fixed predicted probability for dominated choices).

7 Application: Procedural Heterogeneity in Risky Choice

This section estimates procedural heterogeneity in risky choice using the `choices13k` dataset. We first verify the identification conditions on the data and establish out-of-sample predictive performance. We then present the estimated behavioral decomposition - responsibility weights, ablation indices, and concentration measures - followed by an econometric cross-check via the two-step estimator. Finally, we report comparative statics in rule responsibility along menu primitives and portability to an independent dataset. The responsibility weights w_f and context-dependent patterns reported below are *population-level* objects: they describe how the fitted mixture varies across menus in a dataset aggregating choices across many individuals. Without individual-level panel data, within-individual and between-individual components cannot be separated; mechanism-level statements should be read as describing population-level reallocation.

7.1 Identification diagnostics

We evaluate diagnostics D1–D3 on the full Choices13k dataset.

D1. 9,831 of 9,831 menus (100.0%) are two-sided, confirming that the log-odds representation (9) is well-defined on virtually the entire sample.

D2. Table 1 reports per-rule coverage and side-variation. All ten non-attention rules switch sides, and all but one (REG, 30%) are decisive on at least 41% of menus, contributing sign-varying rows to the $H^{(k)}$ matrices that drive condition (G1). The attention rules (A1, A2) are each confined to a single side by construction.

D3. Table 2 evaluates the rank conditions (G1) and (G2) of Corollary 2 on the baseline gate features $z(A) \in \mathbb{R}^{12}$. In the Choices13k data, the 12-dimensional features are essentially unique across menus, so exact-equality cells are singletons. We supplement exact equality with k -means

Table 1: Rule-level coverage and side-variation (D2). For each rule f , N_{act} is the number of menus where f is decisive, $\Pr(L \mid \text{act})$ and $\Pr(R \mid \text{act})$ are the conditional left/right recommendation frequencies. Rules that take both sides contribute sign-varying rows to $H^{(k)}$, supporting condition (G1).

Rule	N_{act}	$\Pr(\text{act})$	$\Pr(L \mid \text{act})$	$\Pr(R \mid \text{act})$	Switches
MMN	9,584	0.975	0.294	0.706	✓
MMA	9,668	0.983	0.580	0.420	✓
MMX	9,688	0.985	0.739	0.261	✓
MAP	9,512	0.968	0.410	0.590	✓
SAL	9,831	1.000	0.485	0.515	✓
SAL2	4,057	0.413	0.509	0.491	✓
REG	2,957	0.301	0.543	0.457	✓
REGMED	8,661	0.881	0.446	0.554	✓
DIS	4,773	0.486	0.322	0.678	✓
DISMED	4,773	0.486	0.336	0.664	✓
A1	9,831	1.000	1.000	0.000	
A2	9,831	1.000	0.000	1.000	

Table 2: Global identification verification (D3). Conditions (G1) and (G2) of Corollary 2 are checked on the Choices13k data using k -means clustering on interpretable z -features ($d = 11$).

Condition	Value	Status
Effective feature dimension d_{eff}	11	
(G1) Cells with $\text{rank}(H^{(k)}) = \mathcal{F} - 1$	41 / 12 needed	✓
(G2) $\text{rank}([1, z])$	12 / 12 needed	✓
Globally identified		✓

clustering on $z(A)$, grouping menus into 50 cells.⁸ Of these, 41 cells achieve $\text{rank}(H^{(k)}) = |\mathcal{F}| - 1$, well above the $d_{\text{eff}} + 1 = 12$ needed for (G1). Among the G1-passing cells, the augmented centroid matrix has full affine rank, satisfying (G2). Both conditions are supported under approximate binning. The rank conditions are structurally stable: because the relevant singular values are well above the SVD tolerance ($10^{-8} \times \sigma_1$), small perturbations in $\hat{r}(A)$ do not change the ranks.

We note that the k -means diagnostic rests on an approximation that lies outside the formal identification theory: Theorem 1 requires menus in a cell to share the *exact* feature value x , whereas clustering only ensures approximate homogeneity within each cell. This is a standard finite-sample device analogous to binning in semiparametric estimation, and its validity depends on $\omega(x)$ varying smoothly over the feature support. The overidentification J -test reported in Section 7.8 provides a complementary, estimation-based check on the adequacy of the gate restriction that does not rely on exact-equality cells.

⁸The number of clusters (50) is chosen so that each cell contains at least $|\mathcal{F}| - 1$ menus while keeping within-cell feature variation modest.

7.2 Predictive validation

Before examining the behavioral decomposition, we verify that the MSE-fitted model predicts well out of sample. Table 3 reports mean test MSE across 50 random train/test splits, with learning-rate selection as described in Section 6. The rule-gating predictor substantially outperforms the standard structured models (Neural EU/PT/CPT and Value-Based) and the flexible Context-Dependent model, closing nearly all of the gap to the strongest benchmark (MOT), providing strong support for the identified decomposition.

Concretely, rule-gating improves on the Value-Based model and on all Neural EU/PT/CPT baselines by a substantial margin. These gains indicate that a small repertoire of transparent “lines of conduct,” combined with a flexible gate that learns when each procedure applies, captures substantial regularity in the data that is missed by standard preference-based architectures. Rule-gating also substantially outperforms the flexible Context-Dependent model. Only the Mixture of Theories (MOT) achieves a marginally lower MSE, with the gap closing to about 2.5% of the MSE level; this is consistent with the fact that MOT allows richer menu interactions than any fixed rule library, but indicates that the structured decomposition captures nearly all of the exploitable variation.⁹

Figure 1a visualizes the comparison with split-variability bands; rankings are stable across splits. Figure 1b reports a learning-curve diagnostic. Rule-gating outperforms MOT at small training fractions and remains essentially tied through moderate fractions; MOT pulls slightly ahead only above roughly 70% of the training data, consistent with its larger number of free parameters requiring larger samples to pay off. Rule-gating consistently outperforms both the context-dependent and value-based networks across all fractions, confirming that a small rule repertoire captures variation beyond a single preference representation. Notably, rule-gating achieves strong performance even with limited data: at 10% of the training sample it already outperforms the value-based network at full sample, reflecting the efficiency gains from the structured rule library.

The trial-weighted metric MSE_w (Table 3) preserves all pairwise orderings. Appendix Tables A.2 and A.3 report split-level comparisons and split-variability intervals.

Interpretability–accuracy tradeoff. A gradient-boosted tree ensemble (GBT) trained on raw lottery summary statistics achieves MSE 0.0096 (Appendix Table A.7), meaningfully below both rule-gating (0.0117) and MOT (0.0114). The interpretability cost of the RRM is therefore non-trivial. We view this as a worthwhile tradeoff because the RRM’s interpretability is *structural*, not post-hoc: for each menu, it decomposes the prediction into contributions from named behavioral procedures with economically interpretable weights. Post-hoc explainability tools identify which *features* matter but cannot decompose predictions into named *procedures*. This structural decomposition, together with the identification guarantees of Section 3, is what permits the mechanism-level analysis that follows.

⁹A caveat on feature sets: the rule-gating model’s effective inputs include both the 12-dimensional gate features $z(A)$ and the 24-dimensional rule activity and recommendation indicators, which are nonlinear functions of the lottery primitives. The neural benchmarks operate on the raw 40-dimensional encoding $\psi(A)$ with small, generic architectures. The comparison therefore does not hold features fixed; the feature-based baseline comparison in Appendix L (Table A.7) provides the closest feature-controlled evaluation.

Table 3: Out-of-sample predictive performance (50 random splits). Learning rates are selected by inner-fold validation MSE (Pass A); test MSE and MSE_w are evaluated at the selected learning rate on the held-out test set (Pass B). MSE_w denotes the trial-weighted MSE defined in (21).

Model	Mean MSE	SD	Mean MSE_w	Best LR
MOT	0.01139	0.00056	n.a.	0.001
Rule-gating	0.01168	0.00049	0.01155	0.010
Context-dependent	0.01344	0.00081	0.01330	0.010
Value-based	0.01921	0.00081	0.01904	0.010
Neural PT	0.02064	0.00085	0.02050	0.010
Neural CPT	0.02145	0.00093	0.02134	0.010
Neural EU	0.02215	0.00085	0.02205	0.010

Note: [†]MOT learning rate is selected by test MSE following the published protocol of Peterson et al. (2021) (see Section 6.4); the HURD framework does not produce per-menu predictions, so MSE_w is unavailable for MOT in cross-validation.

7.3 Responsibility weights w_f

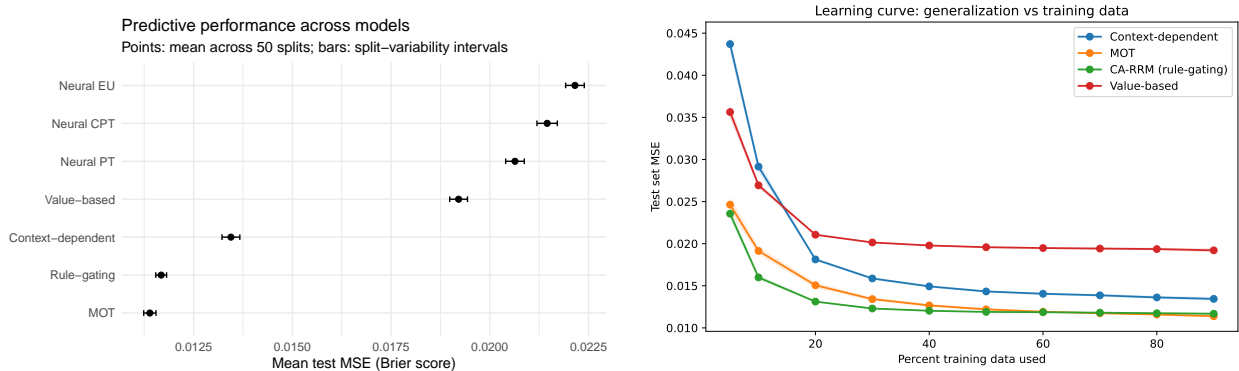
Figure 2 reports the fitted rule-responsibility weights w_f for the full 12-rule model, computed as average *conditional-on-activity* responsibilities:

$$w_f = \mathbb{E}_A \left[\tilde{q}_f(A; \hat{\theta}) \right], \quad \tilde{q}_f(A; \theta) = \frac{q_f(A; \theta) A_f(A)}{\sum_{g \in \mathcal{F}} q_g(A; \theta) A_g(A)}.$$

Recall that w_f measures the average share of decision mass attributed to rule f among *decisive rules*. We refer to w_f as the *responsibility* (or attribution) weight of rule f , since it reflects the fraction of the predicted choice probability that can be attributed to that rule in the fitted mixture, rather than a direct observation of which rule a decision-maker “uses.”

Two patterns stand out. First, the attention rules A1 and A2 absorb the two largest shares of effective responsibility ($w_{A1} \approx 0.280$ and $w_{A2} \approx 0.260$), with a combined attention weight of about 54%. This is expected: the attention rules are decisive on essentially all menus and serve as a catch-all channel. Among the other rules, SAL (most salient comparison, 9.4%), REG (regret, 7.4%), MAP (modal payoff, 6.0%), MMX (aspiration, 5.2%), and MMN (security, 5.1%) carry the largest responsibility weights. Second, because multiple rules are typically active on the same menu (on average, about 5.8 rules are both active and consistent with the majority choice direction), these responsibility weights reflect the outcome of competition among substitutable procedures rather than mechanical assignment to the only available rule.

It is useful to separate the library into two conceptual channels. The *structured rules* (MMN, MMA, MMX, MAP, SAL, SAL2, REG, REGMED, DIS, DISMED) encode distinct behavioral mechanisms that generate non-trivial, menu-dependent recommendations. The *attention channel* (A1 and A2) captures inattention, hasty responding, or trembling: A1 always recommends left and A2 always recommends right, regardless of lottery content. These attention rules absorb roughly half of effective responsibility, reflecting the prevalence of default-like behavior in the online (MTurk) environment. Because the marginal left-choice frequency is $\bar{p} \approx 0.510$ (essentially one-half), this weight cannot be explained by aggregate position bias; rather, the gate allocates attention weight in a menu-dependent way. Part of this weight may, however, reflect absorption of residual prediction



(a) Mean test MSE across 50 random splits (split-variability band).

(b) Learning curve: test MSE vs. training fraction (split-variability band).

Figure 1: Predictive performance. Panel (a) compares out-of-sample MSE across models. Panel (b) reports the learning curve, plotting test-set MSE as a function of the percent training data used.

error by always-active rules rather than a cleanly identified behavioral channel. Our interpretability claims concern the *structured rules conditional on the inattention channel*. Section 8.2 confirms that mechanism patterns persist when the attention channel is removed entirely.

The Herfindahl index $\text{HHI}(F) = \sum_f w_f^2 \approx 0.173$ yields an effective number of rules $N_{\text{eff}} = 1/\text{HHI} \approx 5.8$, reflecting the concentration of responsibility on the attention channel; among the ten structured rules alone, weight is more evenly spread.

7.4 Rule concentration

We next quantify which procedures are necessary for predictive fit. Figure 3a reports the ablation index $\phi(f)$, the relative change in test MSE when rule f is removed from the full library and the gate is retrained on the reduced set. We ablate each of the 10 behavioral rules (excluding attention rules A1/A2, which serve a structural role ensuring decisiveness at every menu). A small subset of rules accounts for most of the ablation impact: removing SAL2 or SAL produces the largest deterioration, followed by REGMED and REG. MAP, MMX, and MMN have moderate impacts, while DIS/DISMED have small impacts. Notably, SAL2 has a relatively high ablation impact despite carrying a lower average responsibility weight than SAL; this illustrates the distinction between w_f (average usage) and $\phi(f)$ (marginal predictive contribution), and suggests that the second-most-salient comparison provides incremental content not replicated by other rules. MMA has a slightly *negative* ablation index, indicating that removing this low-weight rule marginally improves fit—a standard regularization effect when a near-redundant rule is dropped.

Ablations identify rules that matter for accuracy, but they do not indicate whether a rule acts as a *unifier* (concentrating effective responsibility on a small repertoire) or as a *substitute* that diversifies the fitted mixture. To capture this, in Figure 3b, we report the relative change in the effective number of rules $\sigma_N(f)$. We find that $\sigma_N(f)$ is negative for all non-attention rules except REG, which has a small positive value. Removing REG slightly *increases* the effective number of rules, reflecting its specialized role: REG is active on only about 30% of menus, and its removal frees weight to spread more evenly across the broadly active rules. For all other rules, $\sigma_N(f) < 0$: removing a rule concentrates the mixture. The magnitude is largest for the same procedures that

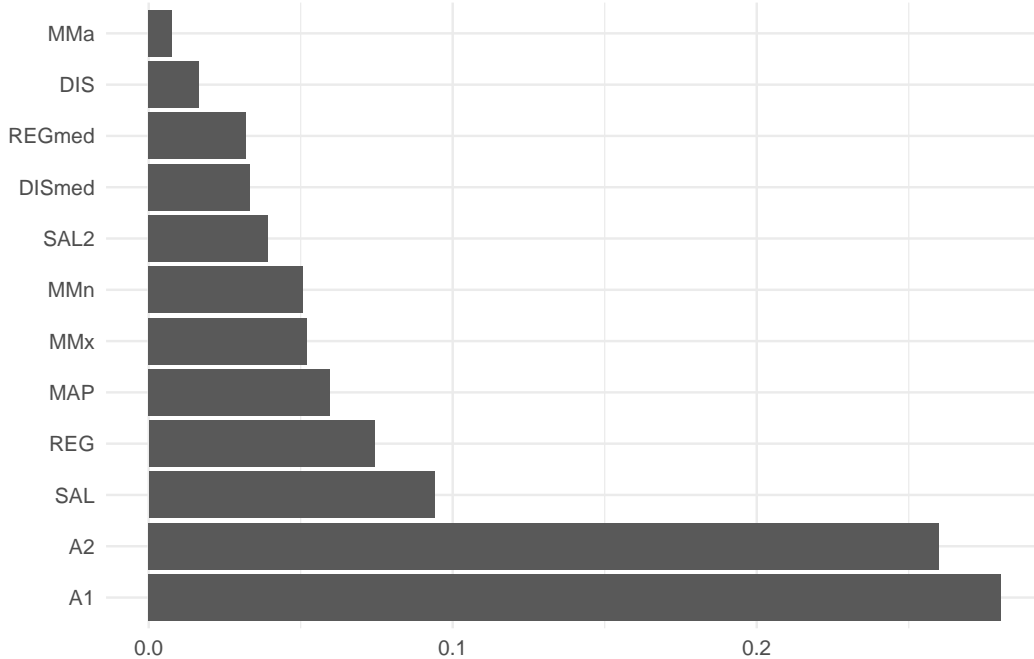


Figure 2: Rule responsibility weights w_f for the full 12-rule library. Each w_f is the average share of predicted choice probability attributed to rule f among decisive rules.

have large ablation impacts, indicating that these rules both attract mass and shape the overall mixture structure.

Overall, salience-based and regret-type comparisons account for the largest ablation impacts, as evidenced by their large $\phi(f)$, while the responsibility weights w_f additionally highlight SAL and REG as the most prominent structured rules. Most remaining rules act as substitutes that diversify the fitted mixture, as indicated by their negative $\sigma_N(f)$ values. Appendix Table A.4 reports split-variability intervals for the absolute ablation effect ΔMSE , confirming that the main rankings are stable. More broadly, fold-level stability of the decomposition objects is reported in Appendix Table A.5: the rule rankings by w_f are highly stable across independent training samples (mean Spearman 0.93); $\phi(f)$ rankings show moderate stability (mean Spearman 0.44), reflecting the greater sensitivity of ablation effects to sample composition. This decomposition provides a transparent characterization of which bounded-rationality mechanisms are empirically relevant in a large dataset of choice under risk—a level of structural interpretability not available from the more flexible predictors.

Library coverage

Figure 4 shows that menus pinning down a unique decisive rule are rare ($\Pr[N_{\text{cons}}(A) = 1] \approx 0.16\%$), while the average number of rules both active and consistent with the majority direction is $\mathbb{E}[N_{\text{cons}}(A)] \approx 5.8$, with about 9.5 rules active per menu. The gate therefore learns selection among genuinely competing procedures.

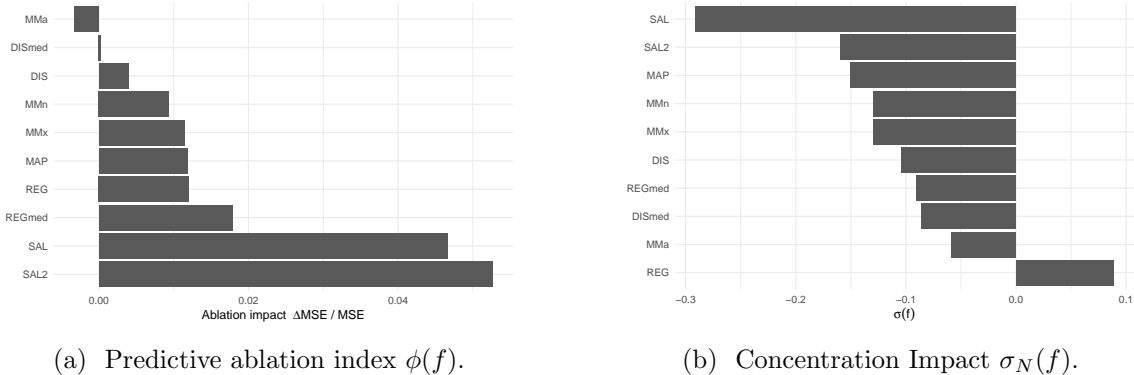


Figure 3: Rule diagnostics: ablation of each behavioral rule from the full 12-rule library. Error bars show split-variability intervals ($\pm 1.96 \times \text{SE}$) from fold-to-fold variability across 50 CV splits.

7.5 Comparative statics in rule responsibility

The figures in this section plot *effective responsibility weights* $\tilde{q}_f(A; \theta)$, which condition on rule activity (Equation (5)). Changes in \tilde{q}_f across menus reflect two channels: (i) genuine shifts in the latent gate propensity $q_f(A; \theta)$ and (ii) mechanical denominator effects from the composition of the active set \mathcal{F}_A , which varies across menus. To verify that the patterns documented below are not artifacts of the activity normalization, Appendix Figures A.3–A.4 reproduce the comparative statics using the latent gate outputs $q_f(A; \theta)$ directly (before conditioning on activity). The qualitative patterns are preserved: the latent gate itself shifts weight across rules in the same directions as the effective decomposition, confirming that the reported patterns reflect genuine variation in the learned gate rather than mechanical composition effects.

Complexity

A central motivation for rule-gating is that a fixed decision rule is too coarse to account for behavior across the wide range of menus in `choices13k`. The substantive hypothesis is therefore not merely that people are noisy, but that they adaptively select different procedures across menus. To connect this hypothesis to the emerging literature on complexity and procedure choice, we rely on an objective notion of menu complexity that is defined directly from the two lotteries in the menu and is available ex ante. This notion is designed to capture when a choice problem requires trading off state-by-state advantages and disadvantages across the two options—precisely the situations where different heuristics can plausibly disagree and where a gate has something non-trivial to learn.

In binary lottery choice, a particularly natural notion is *tradeoff complexity*. Formally, for a menu $A = \{L^1, L^2\}$, let F_1 and F_2 denote the cumulative distribution functions of the two objective lotteries (after placing their supports on a common ordered grid). Define the CDF distance

$$\Delta_{\text{CDF}}(A) := \int_{\mathbb{R}} |F_1(x) - F_2(x)| dx,$$

and the associated *excess dissimilarity*

$$d(A) := \Delta_{\text{CDF}}(A) - |EV(L^1) - EV(L^2)|.$$

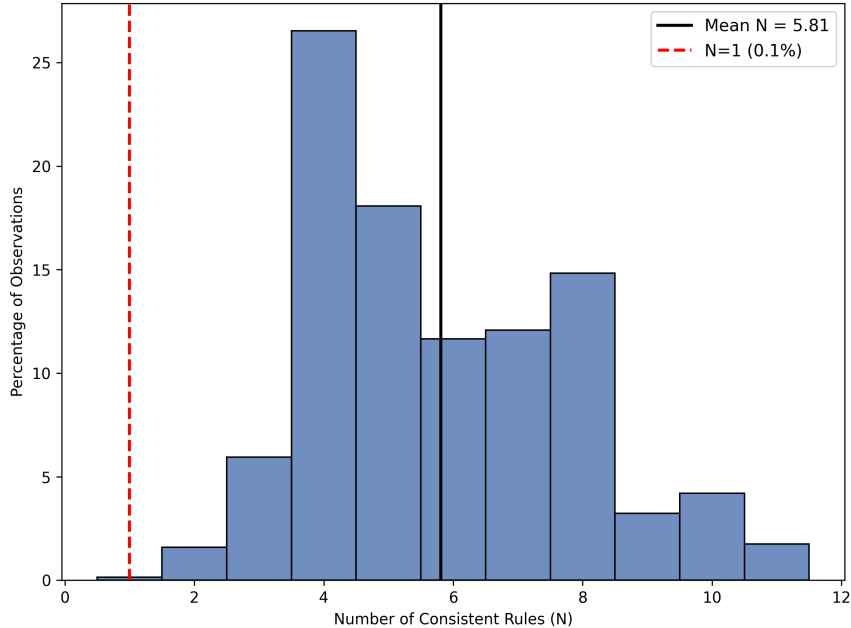


Figure 4: The histogram plots $N_{\text{cons}}(A)$.

The subtraction removes the mechanical effect of a pure value gap and isolates the extent to which the two lotteries “cross” in payoff space, i.e., the extent to which the comparison requires genuine tradeoffs rather than a near-unanimous ordering. In the empirical analysis we work with the log-transformation $\text{TC}(A) := \log(1 + d(A))$ and plot mean effective responsibility weights across complexity deciles.

Figure 5 shows clear and interpretable shifts in rule selection along tradeoff complexity. As $\text{TC}(A)$ increases, the two attention rules ($A1/A2$) display a pronounced increase in mean effective weight, consistent with the view that more complex menus are associated with a greater reliance on coarse inattention in the learned CA-RRM. Among the structured procedures, the most striking pattern is REG (regret): it carries its highest weight in the lowest-complexity deciles and drops steeply to near zero at high complexity, indicating that regret-type evaluation is concentrated on simple menus where state-by-state comparison is tractable. SAL (salience) rises with complexity, while MAP (modal payoff) displays an inverted-U pattern, peaking at moderate complexity and declining at both extremes. MMX (aspiration) shows a mild increase across deciles. Overall, increasing tradeoff complexity tilts the fitted mixture away from evaluative comparisons (regret, modal outcome) and toward attention-based procedures and salience.

Risk

A second natural driver is the risk profile of the menu. Different procedures emphasize different aspects of risk, such as dispersion, downside exposure, and sensitivity to rare events. As a first-pass risk descriptor available directly from the menu, we consider the absolute asymmetry in dispersion across the two lotteries,

$$\text{RiskAsym}(A) := |\sigma(L^1) - \sigma(L^2)|,$$

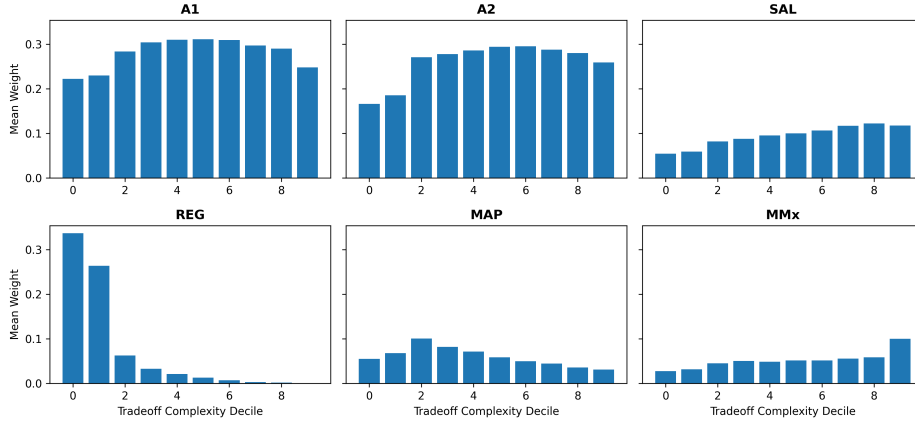


Figure 5: Mean effective responsibility weights across deciles of tradeoff complexity $TC(A)$ for the highest-weight rules.

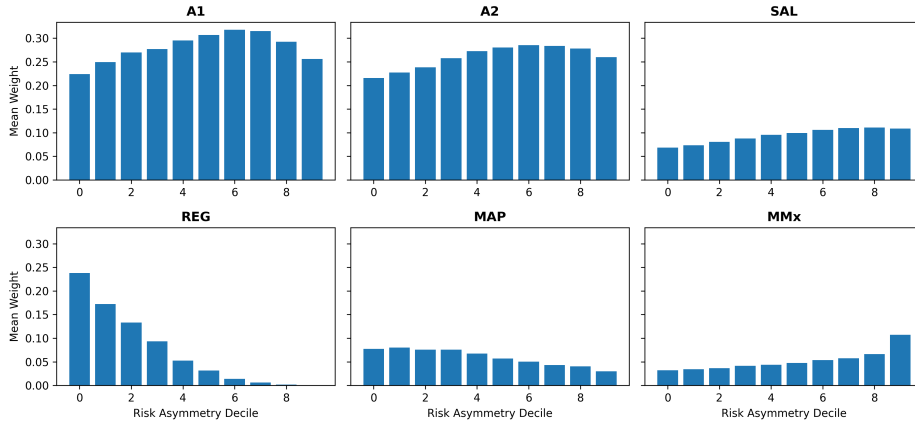


Figure 6: Mean effective responsibility weights across deciles of risk asymmetry $RiskAsym(A)$ for the highest-weight rules.

where $\sigma(L)$ denotes the standard deviation of lottery L . This measures how different the two lotteries are in terms of spread, regardless of which lottery is riskier. Figure 6 plots mean responsibility weights across deciles of this measure.

Figure 6 provides a complementary view based on dispersion asymmetry. The most striking pattern involves REG (regret): its weight is highest when the two lotteries have similar dispersion (low asymmetry) and declines steeply as the gap in spread widens. By contrast, the attention defaults A1 and A2 increase monotonically with risk asymmetry, suggesting that large differences in spread push the gate toward inattention. SAL and MMx show mild increases, while MAP declines gently. Thus, in menus where the two options differ markedly in spread, the gate shifts mass away from regret-type evaluation and toward attention defaults.

These diagnostics show that rule selection varies systematically with salient menu primitives: along complexity, the mixture tilts toward inattention and salience-based comparison and away from regret-type and modal-outcome evaluation; along dispersion asymmetry, regret-type comparison

declines steeply while attention defaults rise. Menu-dependent selection across a small repertoire of procedures is economically meaningful.

7.6 Completeness and Restrictiveness

We supplement the absolute MSE comparisons with two diagnostics: *completeness* (how much of a flexible benchmark’s variation is captured by a structured model) and *restrictiveness* (how tightly a model class constrains the mappings it can fit). Together, they help separate performance gains reflecting substantive structure from gains due to sheer flexibility.

ML Completeness Score

Following Peysakhovich and Naecker (2017), Fudenberg and Puri (2022), and Fudenberg et al. (2022), we define the ML completeness of model g relative to Neural EU (baseline) and MOT (flexible benchmark):

$$\text{Comp}(g) := \frac{\text{MSE}(g_{\text{EU}}) - \text{MSE}(g)}{\text{MSE}(g_{\text{EU}}) - \text{MSE}(g_{\text{MOT}})}. \quad (24)$$

By construction, $\text{Comp}(g_{\text{EU}}) = 0$ and $\text{Comp}(g_{\text{MOT}}) = 1$; values in $(0, 1)$ indicate partial recovery. Figure 7a shows that rule-gating recovers approximately 97% of the baseline-to-MOT gap, compared to $\approx 27\%$ for the Value-based architecture, indicating that the identified decomposition captures nearly all of the structure captured by the most flexible benchmark.

Restrictiveness

A complementary question is *restrictiveness*: how tightly a model class constrains the set of menu-to-choice mappings it can fit (Selten, 1991; Fudenberg et al., 2026). Following Fudenberg et al. (2026), we operationalize this by asking how well a model can fit structureless targets. Let π be a random permutation of the training menus \mathcal{T} and define permuted targets $\hat{p}^\pi(A) := \hat{p}(\pi(A))$. For each model class $g(\cdot; \theta)$, we re-estimate parameters on the permuted targets using the same architecture, the same learning rate selected from the main analysis (Table 3), and the same training horizon—but *without* re-running the inner learning-rate search. We define *permutation-fit restrictiveness* as the ratio of the model’s in-sample MSE on permuted targets to the error of the best constant predictor for those targets:

$$\text{Restr}(g) := \mathbb{E}_{\mathcal{T}, \pi} \left[\frac{\text{MSE}_{\text{train}}^\pi(g)}{\text{MSE}_{\text{train}}^\pi(\text{const})} \right], \quad (25)$$

where the expectation averages over the same $K = 50$ train/test splits and $P = 10$ independent permutations per split. Values near 1 indicate that the model cannot fit permuted targets better than a constant predictor (highly restrictive); values well below 1 indicate that it can absorb structureless patterns (weakly restrictive). In finite samples $\text{Restr}(g)$ can slightly exceed 1 when optimization or regularization prevents the model from matching the constant baseline on permuted data.

Results. Figure 7b shows that MOT is markedly less restrictive ($\text{Restr} \approx 0.2$), while rule-gating and the neural utility benchmarks cluster near 1. Figure 8 plots models in the (completeness, restrictiveness) plane: rule-gating occupies the upper-right region, capturing a large share of the

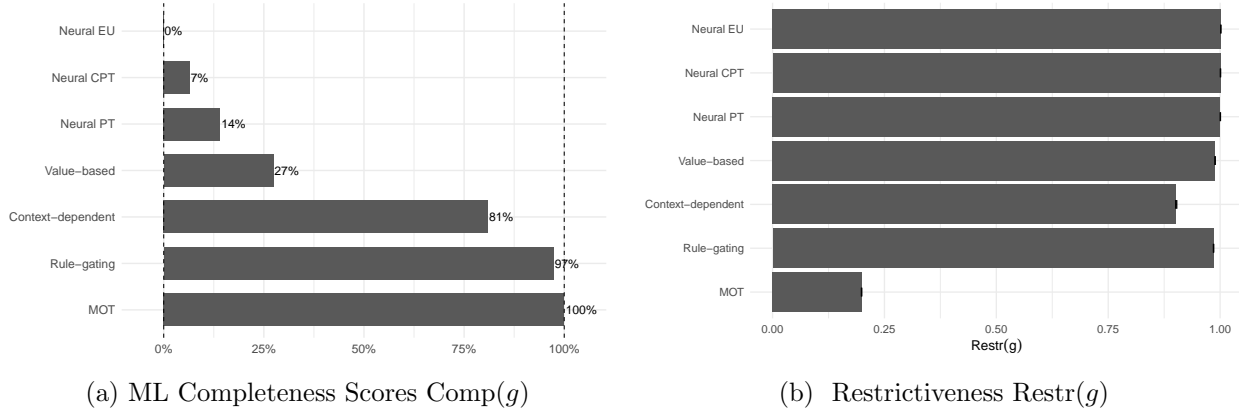


Figure 7: Completeness and Restrictiveness.

variation captured by flexible benchmarks while retaining strong discipline against fitting arbitrary mappings.

7.7 Portability

Finally, a central motivation for interpretable decision procedures is that they are intended to capture stable regularities of behavior, not merely to interpolate within a single dataset. A natural final check is therefore *portability*: does a predictor trained on one large-scale choice environment retain predictive content when exported - without re-tuning - to an independent dataset with different subjects and a different menu sample?

To assess portability, we evaluate models trained on `choices13k` (Peterson et al., 2021) on the independent CPC18 dataset (Erev et al., 2017; Plonsky et al., 2017).¹⁰ We restrict to risk problems, yielding 686 subjects, $|\mathcal{A}^{\text{CPC}}| = 180$ distinct menus, and 354,400 total trials.¹¹

For each model, we freeze `choices13k`-estimated parameters and evaluate on CPC18 menus using

$$\text{MSE}_{\text{CPC}}(g_{\rightarrow}) := \frac{1}{|\mathcal{A}^{\text{CPC}}|} \sum_{A \in \mathcal{A}^{\text{CPC}}} \left(g_{\rightarrow}(A) - \hat{p}_{\text{CPC}}(A) \right)^2. \quad (26)$$

The outcome rescaling factor is computed from `choices13k` and applied identically to CPC18.¹² No hyperparameters are tuned on CPC18. Because CPC18 records individual-level trial data, we also evaluate at the trial level using the Brier score and Bernoulli log-loss.

Portability results. Table 4 reports results. MOT—the best in-sample performer—deteriorates sharply under transfer, suggesting that much of its advantage is dataset-specific. Rule-gating retains strong predictive content: CPC18 MSE 0.0148, ahead of the context-dependent model (0.0173) and far ahead of the structured neural benchmarks (≈ 0.032). Rule-gating therefore offers the best portability among all models *with* an interpretable behavioral decomposition.

¹⁰The data can be downloaded at <https://cpc-18.com/data/>.

¹¹In addition to menu-level aggregation, we also report a trial-weighted evaluation.

¹²Both datasets use a common monetary unit, so the rescaling simply puts outcomes on a common numerical scale.

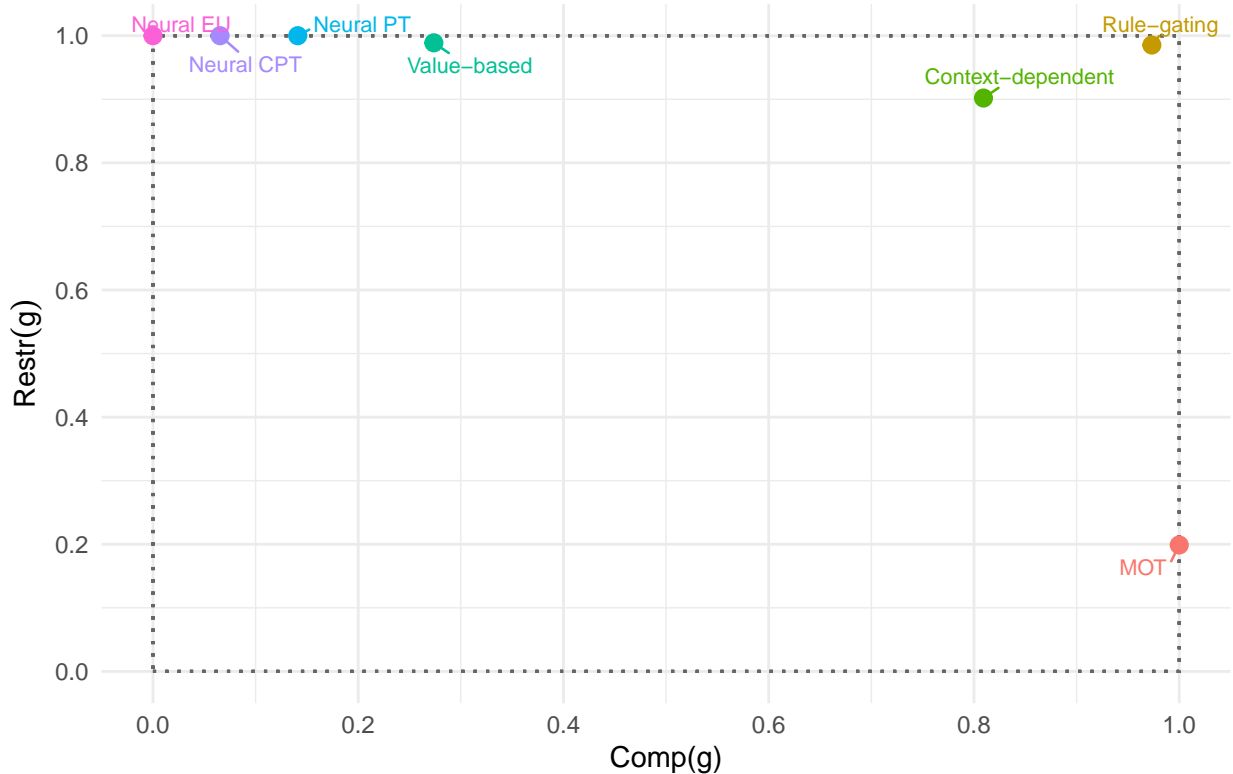


Figure 8: Completeness–restrictiveness plot. The horizontal axis is ML completeness (Equation (24)); the vertical axis is permutation-fit restrictiveness (Equation (25)).

7.8 Two-step econometric estimates

Table 5 reports the results of the two-step econometric estimator described in Section 5, applied to the same data. The first stage groups menus into 47 cells by k -means on $z(A)$ and recovers cellwise normalized weights $\hat{\omega}(x^{(k)})$ via constrained least squares on the $H^{(k)}$ matrices (minimizing $\|H^{(k)}\omega\|^2$ subject to $\omega_{f_0} = 1, \omega_f \geq \varepsilon$). The second stage regresses $\log \hat{\omega}_f(x^{(k)})$ on the cell centroids $[1, x^{(k)}]$ to recover the affine gate coefficients $(\hat{\alpha}_f, \hat{\beta}_f)$. This implementation involves two practical modifications relative to the estimator analyzed in Theorem 3: approximate binning via k -means in place of exact common-feature cells, and positivity constraints on the first-stage weights. Both are standard: binning is asymptotically innocuous under smooth variation of $\omega(x)$, and the positivity constraints do not bind when true weights are strictly positive. The two-step results should accordingly be read as an econometric cross-check motivated by the identification theory, rather than as carrying the full inferential status of Theorem 3.

The two-step responsibility weights w_f show moderate-to-good agreement with the MSE-fitted decomposition: Spearman rank correlation is 0.70 (Pearson = 0.40). SAL, REG, and A2 appear in the top five under both estimators, but point estimates and ordinal ranks differ. The most notable discrepancy involves the attention rules: A1 carries the largest MSE weight ($w_f = 0.28$) but drops to fifth under the two-step procedure ($w_f = 0.11$), while SAL is the most prominent two-step rule ($w_f = 0.23$) but ranks third under MSE ($w_f = 0.09$). These differences are expected. The attention

Table 4: Portability to CPC18: models trained on `choices13k` and evaluated on CPC18 without re-tuning. Trial-level Brier score and log-loss use individual choice observations ($n = 354,400$); menu-level MSE aggregates to the menu level ($n = 180$).

Model	Brier _{trial}	LogLoss _{trial}	MSE _{menu}
Rule-gating	0.1952	0.5705	0.0148
Context-dependent	0.1977	0.5763	0.0173
Neural CPT	0.2111	0.6111	0.0319
Neural EU	0.2111	0.6115	0.0318
Neural PT	0.2120	0.6135	0.0325
Value-based	0.2122	0.6146	0.0323
MOT	0.2713	0.7513	0.0943

Note: Brier_{trial} and LogLoss_{trial} evaluate each model’s predicted menu-level probability against individual binary choices. All models are trained once on the full Choices13k sample and evaluated on CPC18 without re-tuning.

rules are one-sided: A1 always recommends L^1 and A2 always recommends L^2 , regardless of the menu. They therefore contribute no within-cell variation in decisive-side patterns — precisely the variation that the first-stage constrained least squares exploits to identify rule weights. Their two-step weights are identified only residually, after the structured rules with genuine recommendation variation have been fit. By contrast, the MSE estimator minimizes prediction error globally and can freely load weight onto the inattention rules.

The overidentification J -test (Table 5, last column) rejects the affine gate restriction at the 1% level for most rules, indicating that the linear-index parameterization $\log \omega_f(x) = \alpha_f + \beta_f^\top z$ is too parsimonious to capture the full pattern of cellwise weight variation. A1 ($J = 26.1$, $p = 0.86$) and MMA ($J = 45.4$, $p = 0.11$) are the exceptions: the former is consistent with attention being approximately constant across feature values, while the latter carries negligible weight under both estimators. This rejection is not unexpected: with 47 cells and $d_{\text{eff}} + 1 = 12$ parameters, the test has 35 degrees of freedom and substantial power against smooth departures from linearity.

Both procedures share the same functional form: $\log(q_f(x)/q_{f_0}(x)) = \alpha_f + \beta_f^\top x$; the softmax is the normalized-probability representation of the affine index, not a separate gate class. The distinction is in the estimator, not the model: the two-step recovers cellwise weights nonparametrically and then fits the affine index via WLS, exposing the overidentifying restrictions that the J -test evaluates, while the MSE procedure optimizes prediction directly over the same parameterization without testing those restrictions. When the J -test rejects—as it does for most rules—the two estimators diverge in interpretation: the two-step estimator recovers cellwise weights with a specification diagnostic, while the MSE estimator yields a pseudo-true predictive projection. The MSE decomposition remains informative as a descriptive summary but should not be read as the exactly identified structural gate unless the affine restriction is supported. Importantly, Theorem 1 is fully nonparametric and does not require an affine gate: the cellwise identification of relative weights holds for any functional form. The J -test rejection therefore suggests that a richer second-step specification—such as a sieve or kernel parameterization—could reduce or eliminate rejection while preserving the first-step identification logic. This is a natural direction for future work.

Table 5: Two-step econometric estimator vs. MSE-fitted responsibility weights w_f . The two-step estimator recovers cellwise rule weights by constrained least squares on $H^{(k)}$, then maps log-weights into affine gate parameters. Bootstrap standard errors (100 resamples) in parentheses. The J -statistic tests the affine gate restriction (χ^2_{35}).

Rule	w_f (two-step)	w_f (MSE)	Difference	J -stat
MMN	0.131 (0.062)	0.051	+0.080	293.2***
MMA	0.000 (0.012)	0.008	-0.008	45.4
MMX	0.170 (0.063)	0.052	+0.118	252.0***
MAP	0.023 (0.062)	0.060	-0.037	357.6***
SAL	0.228 (0.070)	0.094	+0.134	197.0***
SAL2	0.072 (0.034)	0.039	+0.033	210.1***
REG	0.099 (0.030)	0.074	+0.025	152.2***
REGMED	0.039 (0.051)	0.032	+0.007	212.3***
DIS	0.004 (0.022)	0.017	-0.013	186.5***
DISMED	0.001 (0.028)	0.033	-0.032	136.4***
A1	0.109 (0.070)	0.280	-0.171	26.1
A2	0.123 (0.043)	0.260	-0.137	—

Pearson correlation: 0.401; Spearman rank correlation: 0.699
*** $p < 0.01$; H_0 : $\log \omega_f(x)$ is affine in x

8 Further Robustness

We subject the framework to targeted robustness checks addressing library composition, the attention channel, the activity discipline, and the choice of gate features.

8.1 Cross-fitted library restrictions

A potential concern with the rule library is that it was assembled *ex ante* by the researcher, and performance may depend on the particular collection of rules included. To address this, we implement a cross-fitted selection protocol that chooses rule subsets *only on training folds* and evaluates performance out of sample.

Top- k selection. For each CV fold, we fit the full 12-rule model on the training set, rank rules by w_f , select the top- k ($k \in \{3, 5, 7, 12\}$), refit a restricted gate, and evaluate out of sample.

Family selection. We group rules into five families—extremum, salience, regret, disappointment, attention—and select the top- k_{fam} families ($k_{\text{fam}} \in \{1, \dots, 5\}$) by aggregate training-set responsibility.

Table 6 reports results. Restricting to $k = 7$ rules retains the bulk of full-library accuracy; at $k = 3$, retention drops to about 34%, indicating that three rules are too few to span the behavioral variation. Under family selection, two families suffice for strong performance, but a single family does not. Selection is stable across folds (Appendix Table A.6), and the selected rules match the

Table 6: Cross-fitted library restrictions: mean test MSE for top- k and top-family selections from the full 12-rule library. Subsets are chosen on training folds only; performance is evaluated out of sample.

Selection type	k	Mean MSE	SE	Retention (%)
Full (12 rules)	12	0.01199	0.00007	100.0
Top- k	7	0.01266	0.00008	94.4
Top- k	5	0.01388	0.00010	84.2
Top- k	3	0.01992	0.00013	33.9
Full (5 families)	5	0.01198	0.00007	100.0
Top-family	4	0.01214	0.00007	98.6
Top-family	3	0.01324	0.00009	89.5
Top-family	2	0.01484	0.00009	76.1
Top-family	1	0.02304	0.00013	7.6

Note: Retention (%) = $100 \times [1 - (\text{MSE}^k - \text{MSE}^{\text{full}})/\text{MSE}^{\text{full}}]$: 100% means no loss; values below 0% indicate MSE exceeds twice the full-library MSE. Selection is cross-fitted: rule subsets chosen on training data, evaluated on held-out test data.

highest-responsibility rules in the full model, confirming that the library’s predictive content is concentrated on a few core mechanisms.

8.2 Attention-rule removal

As documented in Section 7.3, the attention rules absorb roughly half of effective responsibility, making them an important channel to scrutinize. Table A.1 (Appendix) replicates the main cross-validation with the 10-rule model (excluding A1/A2). The 10-rule model achieves MSE 0.0201, outperforming Neural EU (0.0222), Neural CPT (0.0215), and Neural PT (0.0206), while remaining close to the value-based network (0.0192). This confirms that the attention channel carries substantial predictive content (MSE rises from 0.0117 to 0.0201), but the non-attention rules alone still surpass most structured benchmarks. The context-dependent patterns documented in Figures 5–6 also persist qualitatively under the 10-rule specification; see Appendix E.

8.3 Varying the activity discipline

Our baseline requires strict FSD of the conduct-transformed lotteries. We probe sensitivity by requiring an ε -gap in survival functions for $\varepsilon \in \{0.01, 0.05, 0.10\}$ (strengthening the discipline) and by setting $\varepsilon = -2$ (all 12 rules active on every menu, removing the discipline entirely).

Table 7 reports results. As ε increases, fewer rules are active per menu and MSE rises, reflecting lost discriminatory power. At $\varepsilon = 0.01$, MSE remains close to the baseline, confirming that predictions do not hinge on marginal dominance. Without the discipline ($\varepsilon = -2$), MSE increases only modestly (0.01202 vs. 0.01168): the gate compensates by down-weighting rules lacking a clear signal. The pattern is asymmetric: over-restricting the activity set (high ε) is more costly than under-restricting it, because the former removes genuinely informative rules while the latter only adds noise the gate can suppress. The FSD-based activation is therefore best understood as an *interpretive* discipline ensuring responsibility weights are nonzero only where a rule delivers a decisive

Table 7: Activity discipline robustness: activity statistics and out-of-sample MSE under varied dominance thresholds. The baseline ($\varepsilon = 0$) corresponds to strict FSD; $\varepsilon > 0$ strengthens it; $\varepsilon < 0$ removes it (all rules active).

ε	Mean active rules	Mean overlap	Mean MSE	SD
-2.00	12.00	7.03	0.01202	0.00053
0.00	9.48	5.81	0.01168	0.00049
0.01	9.12	5.56	0.01307	0.00060
0.05	8.99	5.47	0.01364	0.00064
0.10	8.83	5.36	0.01413	0.00066

Note: For $\varepsilon \geq 0$, ε -FSD requires $S^1(z) \geq S^2(z) + \varepsilon$ for all z (with strict inequality somewhere). For $\varepsilon < 0$, all rules are declared active on every menu; recommendations follow standard FOSD where applicable. Mean active rules: average number of decisive rules per menu. Mean overlap: average number of active rules consistent with the majority choice direction. MSE is from the same 50-fold CV protocol as Table 3.

ranking rather than a predictive one.

8.4 Placebo rule library, feature-based baselines, and raw-encoding gate

Three additional robustness checks are reported in Appendix M–N. First, a *placebo test* scrambles each rule’s indicators across menus within complexity strata, preserving marginal activity and recommendation rates but destroying the menu-specific mapping. The placebo library produces substantially higher MSE than the real library (Appendix Table A.8), confirming that the rule indicators carry genuine, menu-specific predictive content.

Second, we benchmark against *feature-based baselines*: a fractional logit and a gradient-boosted tree ensemble (GBT), each trained on rule indicators, summary statistics, or both (Appendix Table A.7). On rule features alone, rule-gating substantially outperforms both baselines, showing that the activity-conditioned gate architecture extracts more from the rule library than standard classifiers (though the gate also conditions on $z(A)$, so the comparison is not purely architectural). GBT on raw summary statistics outperforms all structured models, but provides no behavioral decomposition.

Third, a *raw-encoding gate* variant uses the full 40-dimensional menu representation $\psi(A)$ instead of $z(A)$ (Appendix Figure A.5). It achieves MSE 0.0139, about 19% worse than the baseline $z(A)$ specification (0.0117), confirming that the interpretable summary statistics capture decision-relevant variation without sacrificing accuracy. The global identification conditions (G1)–(G2) are not applicable to this parameterization.

Taken together, these checks confirm that the decomposition is stable, the rule indicators carry genuine predictive content, and the results are not artifacts of the library choice, attention channel, activity discipline, or gate features.

9 Conclusion

This paper studies stochastic choice under latent procedural heterogeneity. We develop a Random Rule Model (RRM) in which observed choice probabilities arise from switching among a small

library of transparent deterministic decision procedures, with environment-dependent rule weights. The main contribution is an identification-and-estimation framework for recovering these latent procedural weights from menu-level choice frequencies. Identification has a two-step structure: within-feature variation in decisive-side patterns identifies relative rule weights, while cross-feature affine richness identifies the gate parameters. A constructive two-step estimator then supports inference for economically meaningful rule-level functionals.

Applied to risky choice, the framework uncovers substantial and systematic procedural heterogeneity. Saliency-based comparisons, regret-type rules, and modal-outcome comparisons receive the largest responsibility weights among structured procedures, and rule responsibility shifts predictably with menu characteristics such as tradeoff complexity and dispersion asymmetry. These comparative statics provide an empirical characterization of risky choice in terms of changing procedure use rather than only reduced-form choice frequencies.

The predictive exercises support the validity of the representation. Rule-gating substantially outperforms structured neural benchmarks, remains highly restrictive under permutation-fit diagnostics, and retains predictive content on an independent dataset. At the same time, the evidence from varying the activity discipline shows that the activity filter is best understood as an attribution operator that restricts behavioral responsibility to rules that are actually decisive, rather than as the primary source of fit.

On the econometric side, the two-step overidentification test rejects the affine gate specification for most rules, indicating that the parsimonious linear-index parameterization does not fully capture how rule weights vary across menu characteristics. Since the first-stage identification is nonparametric, a natural extension is to replace the affine second step with a richer specification. More broadly, the paper suggests that stochastic choice data can be used to recover not only how often each option is chosen, but also how populations reallocate across decision procedures as environments change. This makes procedural heterogeneity a tractable econometric object, and opens the door to applications in consumer choice, dynamic choice, and strategic environments where behavior may be governed by shifting mixtures of transparent rules.

References

- Aguiar, V. H., Kashaev, N., and Ryan, S. P. (2023). Random utility and limited consideration. *Quantitative Economics*, 14(1):1–46.
- Arrieta, G. and Nielsen, K. (2024). Procedural Decision-Making In The Face Of Complexity. Technical report.
- Aumann, R. J. (2008). Rule-rationality versus act-rationality. Discussion Paper Series dp497, The Federmann Center for the Study of Rationality, the Hebrew University, Jerusalem.
- Bordalo, P., Gennaioli, N., and Shleifer, A. (2012). Saliency Theory of Choice Under Risk. *The Quarterly Journal of Economics*, 127(3):1243–1285.
- Cattaneo, M. D., Ma, X., Masatlioglu, Y., and Suleymanov, E. (2020). A random attention model. *Journal of Political Economy*, 128(7):2796–2836.
- Cherepanov, V., Feddersen, T., and Sandroni, A. (2013). Rationalization. *Theoretical Economics*, 8(3):775–800.

- Enke, B. and Shubatt, C. (2023). Quantifying lottery choice complexity. Working Paper 31677, National Bureau of Economic Research.
- Erev, I., Ert, E., Plonsky, O., Cohen, D., and Cohen, O. (2017). From anomalies to forecasts: Toward a descriptive model of decisions under risk, under ambiguity, and from experience. *Psychological Review*, 124(4):369–409.
- Erev, I., Ert, E., Roth, A. E., Haruvy, E., Herzog, S. M., Hau, R., Hertwig, R., Stewart, T., West, R., and Lebiere, C. (2010). A choice prediction competition: Choices from experience and from description. *Journal of Behavioral Decision Making*, 23(1):15–47.
- Fudenberg, D., Gao, W., and Liang, A. (2026). How flexible is that functional form? quantifying the restrictiveness of theories. *The Review of Economics and Statistics*, 108(1):194–209.
- Fudenberg, D., Kleinberg, J., Liang, A., and Mullainathan, S. (2022). Measuring the completeness of economic models. *Journal of Political Economy*, 130(4):956–990.
- Fudenberg, D. and Liang, A. (2020). Machine learning for evaluating and improving theories. *ACM SIGecom Exchanges*, 18(1):4–11.
- Fudenberg, D. and Puri, I. (2022). Simplicity and probability weighting in choice under risk. *AEA Papers and Proceedings*, 112:pp. 421–425.
- Halevy, Y. and Mayraz, G. (2024). Identifying rule-based rationality. *The Review of Economics and Statistics*, 106(5):1369–1380.
- Henry, M., Kitamura, Y., and Salanié, B. (2014). Partial identification of finite mixtures in econometric models. *Quantitative Economics*, 5:123–144.
- Kahneman, D. and Tversky, A. (1979). Prospect theory: An analysis of decision under risk. *Econometrica*, 47(2):263–291.
- Kitamura, Y. and Stoye, J. (2018). Nonparametric analysis of random utility models. *Econometrica*, 86(6):1883–1909.
- Liang, A. (2025). Using machine learning to generate, clarify, and improve economic models. Papers 2508.19136, arXiv.org.
- Loomes, G. and Sugden, R. (1982). Regret theory: An alternative theory of rational choice under uncertainty. *Economic Journal*, 92(368):805–824.
- Loomes, G. and Sugden, R. (1986). Disappointment and dynamic consistency in choice under uncertainty. *Review of Economic Studies*, 53(2):271–282.
- Manzini, P. and Mariotti, M. (2007). Sequentially rationalizable choice. *American Economic Review*, 97(5):1824–1839.
- Manzini, P. and Mariotti, M. (2012). Categorize then choose: Boundedly rational choice and welfare. *Journal of the European Economic Association*, 10(5):1141–1165.
- Manzini, P. and Mariotti, M. (2014). Stochastic choice and consideration sets. *Econometrica*, 82(3):1153–1176.

- Masatlioglu, Y., Nakajima, D., and Ozbay, E. Y. (2012). Revealed attention. *American Economic Review*, 102(5):2183–2205.
- McFadden, D. and Richter, K. (1991). Stochastic rationality and revealed stochastic preference. In Chipman, J., McFadden, D., and Richter, K., editors, *Preferences, uncertainty, and rationality*, pages 161–186. Westview Press, Boulder.
- McFadden, D. L. (2006). Revealed stochastic preference: a synthesis. In Aliprantis, C. D., Matzkin, R. L., McFadden, D. L., Moore, J. C., and Yann, N. C., editors, *Rationality and Equilibrium*, Studies in Economic Theory, pages 1–20. Springer.
- Papke, L. E. and Wooldridge, J. M. (1996). Econometric methods for fractional response variables with an application to 401(k) plan participation rates. *Journal of Applied Econometrics*, 11(6):619–632.
- Peterson, J. C., Bourgin, D. D., Agrawal, M., Reichman, D., and Griffiths, T. L. (2021). Using large-scale experiments and machine learning to discover theories of human decision-making. *Science*, 372(6547):1209–1214.
- Peysakhovich, A. and Naecker, J. (2017). Using methods from machine learning to evaluate behavioral models of choice under risk and ambiguity. *Journal of Economic Behavior & Organization*, 133(C):373–384.
- Plonsky, O., Erev, I., and Ert, E. (2017). Calibration data for choice prediction competition 2018 (cpc18).
- Plonsky, O., Hazan, T., and Tennenholtz, M. (2016). Psychological forest: Predicting human behavior. *SSRN Electronic Journal*.
- Puri, I. (2025). Simplicity and risk. *The Journal of Finance*, 80(2):1029–1080.
- Rubinstein, A. (1988). Similarity and decision-making under risk (is there a utility theory resolution to the allais paradox?). *Journal of Economic Theory*, 46(1):145–153.
- Salant, Y. and Rubinstein, A. (2008). (a, f): Choice with frames. *The Review of Economic Studies*, 75(4):1287–1296.
- Selten, R. (1991). Properties of a measure of predictive success. *Mathematical Social Sciences*, 21(2):153–167.
- Seror, A. (2026). Decision rules in choice under risk.
- Simon, H. A. (1955). A behavioral model of rational choice. *The Quarterly Journal of Economics*, 69(1):99–118.
- Tversky, A. and Kahneman, D. (1992). Advances in prospect theory: Cumulative representation of uncertainty. *Journal of Risk and Uncertainty*, 5(4):297–323.

Online Appendix

A General Procedural Mixture Framework

This section presents the Conditional Activity Random Rule Model (CA-RRM) and its identification theory in a general discrete choice environment with finitely many alternatives per menu. The binary lottery application in the main text is a special case obtained by setting $|A| = 2$ for all menus and instantiating the dominance preorder as first-order stochastic dominance.

A.1 Choice environment

Let \mathcal{M} denote a finite collection of *menus* (choice sets). Each menu $A \in \mathcal{M}$ is a finite set of alternatives with $|A| = n_A \geq 2$. For each menu A and alternative $i \in A$, let $p(i | A) \in (0, 1)$ denote the population choice probability, with $\sum_{i \in A} p(i | A) = 1$.

Assumption A.1 (Interior probabilities). For every $A \in \mathcal{M}$ and $i \in A$, $p(i | A) > 0$.

This ensures that log-ratios of choice probabilities are well defined.

A.2 Procedural library and activity

Let $\mathcal{F} = \{f_1, \dots, f_F\}$ be a finite library of *deterministic decision procedures* (rules). Each rule $f \in \mathcal{F}$ is equipped with:

- (i) An *activity set* $\mathcal{A}_f \subseteq \mathcal{M}$: the menus at which rule f delivers a strict ranking of alternatives. Define the activity indicator $\mathbf{1}_f(A) := \mathbf{1}\{A \in \mathcal{A}_f\}$.
- (ii) A *recommendation mapping* $r_f : \mathcal{A}_f \rightarrow \bigcup_{A \in \mathcal{M}} A$ such that $r_f(A) \in A$ for each $A \in \mathcal{A}_f$: the unique alternative that rule f recommends at menu A when active.

Activity is determined by an exogenous criterion (e.g., stochastic dominance of perceived lotteries in risky choice, present-value dominance in intertemporal choice, or welfare dominance in allocation problems). The key discipline is that a rule contributes to predicted choice probabilities *only* at menus where it is active.

For each menu A and alternative $i \in A$, define the *recommending set*

$$\mathcal{I}_i(A) := \{f \in \mathcal{F} : \mathbf{1}_f(A) = 1, r_f(A) = i\}, \tag{A.1}$$

the set of active rules that recommend alternative i at menu A . The set of all active rules at A is $\mathcal{F}_A := \bigcup_{i \in A} \mathcal{I}_i(A)$.

A.3 The CA-RRM

A *Conditional Activity Random Rule Model* assigns to each menu A a probability distribution $\{q_f(A)\}_{f \in \mathcal{F}} \in \Delta^{F-1}$ over rules. Define the conditional-on-activity weight of rule f :

$$\tilde{q}_f(A) := \frac{q_f(A) \mathbf{1}_f(A)}{\sum_{g \in \mathcal{F}} q_g(A) \mathbf{1}_g(A)}, \quad (\text{A.2})$$

whenever $\mathcal{F}_A \neq \emptyset$. The CA-RRM choice probability is

$$P(i | A; q) = \sum_{f \in \mathcal{I}_i(A)} \tilde{q}_f(A) = \frac{\sum_{f \in \mathcal{I}_i(A)} q_f(A)}{\sum_{g \in \mathcal{F}_A} q_g(A)}. \quad (\text{A.3})$$

Equation (A.3) expresses predicted choice as a mixture over deterministic rule recommendations, conditional on activity.

A.4 Softmax gating parameterization

The CA-RRM becomes a parametric model when $q(A)$ is generated by a differentiable gate. Let $\psi(A) \in \mathbb{R}^d$ be an observable feature vector for menu A . The *softmax gate* sets

$$q_f(A; \theta) := \frac{\exp(u_f(A; \theta))}{\sum_{g \in \mathcal{F}} \exp(u_g(A; \theta))}, \quad (\text{A.4})$$

where $u_f(A; \theta) := \alpha_f + \beta_f^\top \psi(A)$ is an affine score, and $\theta := \{(\alpha_f, \beta_f)\}_{f \in \mathcal{F}}$ collects all gate parameters.

Substituting (A.4) into (A.3) and canceling the common denominator of the softmax, the CA-RRM choice probability simplifies to

$$P(i | A; \theta) = \frac{\sum_{f \in \mathcal{I}_i(A)} \exp(u_f(A; \theta))}{\sum_{g \in \mathcal{F}_A} \exp(u_g(A; \theta))}. \quad (\text{A.5})$$

This is a *grouped softmax* over active rules, with groups defined by the alternative each rule recommends.

A.5 Normalization

The softmax is invariant to adding a common affine function to all scores: if $u_f \mapsto u_f + a + c^\top \psi$ for all f , the probabilities in (A.5) are unchanged. We therefore impose a location normalization by fixing one baseline rule $f_0 \in \mathcal{F}$ and setting

$$(\alpha_{f_0}, \beta_{f_0}) = (0, \mathbf{0}). \quad (\text{A.6})$$

Let $\vartheta \in \mathbb{R}^K$ denote the vector of free parameters, with $K = (F - 1)(1 + d)$.

A.6 Identification map and sufficient-variation condition

Multi-sided menus. Say that a menu A is *multi-sided* if at least two distinct alternatives are recommended by some active rule:

$$|\{i \in A : \mathcal{I}_i(A) \neq \emptyset\}| \geq 2.$$

Let $\mathcal{M}_{\text{ms}} \subseteq \mathcal{M}$ denote the set of multi-sided menus (the analogue of two-sided menus in the binary case). On menus that are not multi-sided, all active rules agree, so the CA-RRM prediction is 1 for the unanimously recommended alternative regardless of θ ; such menus carry no identifying information.

Log-ratio representation. For each multi-sided menu A , restrict attention to alternatives $i \in A$ with $\mathcal{I}_i(A) \neq \emptyset$ (i.e., alternatives recommended by at least one active rule).¹³ Fix a reference alternative $i_0(A)$ among these. By Assumption A.1 and (A.5), the log-ratios

$$\delta_i(A; \vartheta) := \log \frac{P(i | A; \vartheta)}{P(i_0(A) | A; \vartheta)} = \log \sum_{f \in \mathcal{I}_i(A)} \exp(u_f(A; \vartheta)) - \log \sum_{f \in \mathcal{I}_{i_0(A)}} \exp(u_f(A; \vartheta)) \quad (\text{A.7})$$

are well defined for each covered $i \in A \setminus \{i_0(A)\}$.

Identification map. Stack the log-ratios across all multi-sided menus and non-reference alternatives into a single vector:

$$H(\vartheta) := \left(\delta_i(A; \vartheta) \right)_{A \in \mathcal{M}_{\text{ms}}, i \in A \setminus \{i_0(A)\}} \in \mathbb{R}^D, \quad (\text{A.8})$$

where $D = \sum_{A \in \mathcal{M}_{\text{ms}}} (n_A - 1)$. Observing the population choice probabilities $\{p(i | A)\}$ on multi-sided menus is equivalent to observing $H(\vartheta)$, because the log-ratio transformation is a diffeomorphism from the interior of the simplex to $\mathbb{R}^{n_A - 1}$.

A.7 Global identification theorem

Decisive-side indicators and linear restriction. For each rule f and each alternative $i \in A$, define the decisive-side indicator

$$\kappa_f^i(A) := \mathbf{1}\{f \in \mathcal{I}_i(A)\},$$

¹³Under correct specification, Assumption A.1 implies $P(i | A) > 0$ for all $i \in A$, which requires $\mathcal{I}_i(A) \neq \emptyset$ since (A.5) assigns zero probability to uncovered alternatives. Hence the restriction to covered alternatives is implicit in the joint assumption of correct specification and interior probabilities.

where $\mathcal{I}_i(A)$ is the recommending set from (A.1). For each multi-sided menu A , fix a reference alternative $i_0(A)$ with $\mathcal{I}_{i_0}(A) \neq \emptyset$ and write the odds ratio

$$r_i(A) := \frac{P(i | A)}{P(i_0(A) | A)}, \quad i \in A \setminus \{i_0(A)\}.$$

Define the positive rule weights $\omega_f(x) := \exp(\alpha_f + \beta_f^\top x)$ for $x = \psi(A)$. From (A.5), the model-implied odds ratio satisfies

$$r_i(A) = \frac{\sum_{f \in \mathcal{I}_i(A)} \omega_f(x)}{\sum_{f \in \mathcal{I}_{i_0}(A)} \omega_f(x)}.$$

Cross-multiplying and collecting terms yields, for each non-reference alternative $i \in A \setminus \{i_0(A)\}$,

$$\sum_{f \in \mathcal{F}} \left(\kappa_f^i(A) - r_i(A) \kappa_f^{i_0(A)}(A) \right) \omega_f(x) = 0, \quad (\text{A.9})$$

i.e. $h_i(A)^\top \omega(x) = 0$ where $h_{i,f}(A) := \kappa_f^i(A) - r_i(A) \kappa_f^{i_0(A)}(A)$.

Theorem A.1 (Global identification of the general CA-RRM). *Consider the CA-RRM with affine indices $u_f(A) = \alpha_f + \beta_f^\top \psi(A)$, $f \in \mathcal{F}$. Assume $P(i | A) \in (0, 1)$ for all $i \in A$ and all menus in the support (Assumption A.1), and impose the normalization (A.6). Note that under correct specification, this interior-probability condition implies that every alternative $i \in A$ is recommended by at least one active rule (i.e., $\mathcal{I}_i(A) \neq \emptyset$), since (A.5) assigns zero probability to uncovered alternatives. Let $d = \dim(\psi)$. Suppose there exist $(d + 1)$ feature values $x^{(0)}, \dots, x^{(d)}$ such that:*

(G1) **Within-feature variation in decisive-side patterns:** For each $k \in \{0, \dots, d\}$, stack the row vectors $h_i(A)^\top$ across all multi-sided menus A with $\psi(A) = x^{(k)}$ and all non-reference alternatives $i \in A \setminus \{i_0(A)\}$ into a matrix

$$H^{(k)} := \begin{pmatrix} h_{i_1}(A_1)^\top \\ \vdots \\ h_{i_M}(A_M)^\top \end{pmatrix}.$$

Then $\text{rank}(H^{(k)}) = |\mathcal{F}| - 1$.

(G2) **Affine richness of feature values:** The $(d + 1) \times (d + 1)$ matrix $X := \begin{pmatrix} 1 & (x^{(0)})^\top \\ \vdots & \vdots \\ 1 & (x^{(d)})^\top \end{pmatrix}$ has full rank.

Then the full parameter vector $\{(\alpha_f, \beta_f)\}_{f \in \mathcal{F}}$ is globally identified from the population objects $\{P(i | A), \kappa^i(A), \psi(A)\}$, up to the normalization.

Proof. The proof parallels that of Theorem 1 and Corollary 2 in the main text, extended to the multinomial setting.

Step 1 (from choice probabilities to linear equations). Fix a multi-sided menu A and write $x = \psi(A)$. From (A.5), the choice probability ratio for any non-reference alternative i is

$$r_i(A) = \frac{P(i | A)}{P(i_0(A) | A)} = \frac{\sum_f \kappa_f^i(A) \omega_f(x)}{\sum_f \kappa_f^{i_0(A)}(A) \omega_f(x)}.$$

Cross-multiplying yields the linear restriction (A.9): $h_i(A)^\top \omega(x) = 0$, where the coefficients $h_{i,f}(A) = \kappa_f^i(A) - r_i(A) \kappa_f^{i_0(A)}(A)$ are determined by the decisive-side indicators and the observed odds ratio.

Step 2 (identifying $\omega(x)$ at a fixed feature value up to scale). Fix $k \in \{0, \dots, d\}$. All menus A with $\psi(A) = x^{(k)}$ share the same unknown weight vector $\omega(x^{(k)})$, while the decisive-side indicators may vary across menus even at the same feature value. Stacking all rows $h_i(A)^\top$ from these menus into $H^{(k)}$ gives $H^{(k)} \omega(x^{(k)}) = 0$. By (G1), $\text{rank}(H^{(k)}) = |\mathcal{F}| - 1$, so the nullspace is one-dimensional. Since all entries of $\omega(x^{(k)})$ are positive, the weight vector is identified up to a positive scalar.

Step 3 (pinning down scale using the normalization). Under (A.6), $\omega_{f_0}(x) = \exp(0 + \mathbf{0}^\top x) = 1$ for all x . Imposing $\omega_{f_0}(x^{(k)}) = 1$ uniquely pins the scalar, so $\omega(x^{(k)})$ is uniquely identified for each k .

Step 4 (recovering (α_f, β_f) from identified weights). Fix any rule f . From $\log \omega_f(x^{(k)}) = \alpha_f + \beta_f^\top x^{(k)}$ for $k = 0, \dots, d$, we obtain the linear system $(\log \omega_f(x^{(0)}), \dots, \log \omega_f(x^{(d)}))^\top = X(\alpha_f, \beta_f^\top)^\top$. By (G2), X is invertible, so (α_f, β_f) is uniquely determined. Since f was arbitrary, global identification holds. \square

Remark A.1. The binary application in the main text (Corollary 2) is the special case with $|A| = 2$, where each menu produces a single row $h(A)^\top$ and the odds ratio reduces to $p(A)/(1 - p(A))$.

A.8 Local identification theorem

Remark A.2. Theorem A.1 above establishes global identification under conditions (G1)–(G2), which require that multiple menus share the same feature value. The following local result provides an alternative characterization based on the Jacobian of the identification map. It is particularly relevant when the gate operates on a high-dimensional feature map (such as the raw menu encoding $\psi(A) \in \mathbb{R}^{4M}$) for which the replication condition in (G1) may not hold. See Appendix O for further discussion.

Theorem A.2 (Local identification of the general CA-RRM). *Impose the normalization (A.6) and*

let $\vartheta^* \in \mathbb{R}^K$ be any parameter vector. Define the Jacobian

$$J(\vartheta^*) := \left. \frac{\partial H(\vartheta)}{\partial \vartheta^\top} \right|_{\vartheta=\vartheta^*} \in \mathbb{R}^{D \times K}.$$

- (a) If $J(\vartheta^*)$ has full column rank K , then ϑ^* is locally identified from $\{p(i | A)\}_{A \in \mathcal{M}_{\text{ms}}}$: there exists a neighborhood $U \ni \vartheta^*$ such that $H(\vartheta) = H(\vartheta^*)$ and $\vartheta \in U$ imply $\vartheta = \vartheta^*$.
- (b) If $\text{rank}(J(\vartheta^*)) = r < K$, then the null space $\mathcal{N}(J(\vartheta^*))$ has dimension $K - r$, and H is locally constant to first order along these $K - r$ linearly independent directions. If, additionally, the rank of $J(\vartheta)$ equals r on a neighborhood of ϑ^* , then by the constant-rank theorem the level set $\{\vartheta : H(\vartheta) = H(\vartheta^*)\}$ is locally a smooth embedded submanifold of dimension $K - r$ with tangent space $\mathcal{N}(J(\vartheta^*))$.

Proof. Each score $u_f(A; \vartheta)$ is affine in ϑ , and the log-sum-exp function is C^∞ on \mathbb{R}^n for any $n \geq 1$. Therefore $\delta_i(A; \vartheta)$ in (A.7), being a difference of two log-sum-exp functions composed with affine maps, is C^∞ in ϑ . The identification map H is thus a C^∞ map from \mathbb{R}^K to \mathbb{R}^D .

For part (a): if $J(\vartheta^*) \in \mathbb{R}^{D \times K}$ has rank K , there exist K components of H whose $K \times K$ sub-Jacobian is nonsingular (select any K linearly independent rows of $J(\vartheta^*)$). By the inverse function theorem applied to this square submap, the selected components of H are locally injective at ϑ^* . Since $H(\vartheta) = H(\vartheta^*)$ implies equality of the selected subvector, the full map H is locally injective.

For part (b): the first-order statement follows directly from $\text{rank}(J(\vartheta^*)) = r$: by the rank-nullity theorem, $\mathcal{N}(J(\vartheta^*))$ has dimension $K - r$, and for any $v \in \mathcal{N}(J(\vartheta^*))$, the directional derivative $DH(\vartheta^*) \cdot v = 0$. If, additionally, $\text{rank}(J(\vartheta)) = r$ on a neighborhood of ϑ^* , the constant-rank theorem yields the stronger geometric conclusion that the level set is locally a smooth $(K - r)$ -dimensional submanifold. Without this local constancy assumption, the first-order characterization still holds but the level set may have dimension less than $K - r$. \square

A.9 Closed-form Jacobian

We derive the Jacobian entries in closed form. For each active rule $f \in \mathcal{F}_A$, define the *active-set softmax share* (i.e., the share of rule f in the softmax over all active rules, not conditional on alternative)

$$s_f(A; \vartheta) := \frac{\exp(u_f(A; \vartheta))}{\sum_{g \in \mathcal{F}_A} \exp(u_g(A; \vartheta))}, \quad (\text{A.10})$$

and for each alternative $i \in A$, write $S_i(A; \vartheta) := \sum_{f \in \mathcal{I}_i(A)} s_f(A; \vartheta)$ for the total share allocated to alternative i . Note that $P(i | A; \vartheta) = S_i(A; \vartheta)$.

Proposition A.3 (Jacobian entries). *For any multi-sided menu $A \in \mathcal{M}_{\text{ms}}$, any non-reference*

alternative $i \in A \setminus \{i_0(A)\}$, and any free rule $f \neq f_0$:

$$\frac{\partial \delta_i(A)}{\partial \alpha_f} = \frac{s_f(A) \mathbf{1}\{f \in \mathcal{I}_i(A)\}}{S_i(A)} - \frac{s_f(A) \mathbf{1}\{f \in \mathcal{I}_{i_0}(A)\}}{S_{i_0}(A)}, \quad (\text{A.11})$$

$$\frac{\partial \delta_i(A)}{\partial \beta_f} = \left(\frac{s_f(A) \mathbf{1}\{f \in \mathcal{I}_i(A)\}}{S_i(A)} - \frac{s_f(A) \mathbf{1}\{f \in \mathcal{I}_{i_0}(A)\}}{S_{i_0}(A)} \right) \psi(A)^\top. \quad (\text{A.12})$$

If $f \notin \mathcal{F}_A$ (i.e., f is inactive at A), then $s_f(A) = 0$ and both derivatives vanish.

Proof. From (A.7), $\delta_i(A; \vartheta) = \log N_i(A) - \log N_{i_0}(A)$, where $N_j(A) := \sum_{g \in \mathcal{I}_j(A)} \exp(u_g(A))$. For $f \in \mathcal{I}_i(A)$:

$$\frac{\partial \log N_i(A)}{\partial \alpha_f} = \frac{\exp(u_f(A))}{N_i(A)} = \frac{s_f(A) \cdot Z(A)}{N_i(A)} = \frac{s_f(A)}{S_i(A)},$$

where $Z(A) := \sum_{g \in \mathcal{F}_A} \exp(u_g(A))$ and $S_i(A) = N_i(A)/Z(A)$. For $f \notin \mathcal{I}_i(A)$, the derivative is zero. Combining the contributions from the two log terms and noting $\partial u_f / \partial \beta_f = \psi(A)^\top$ gives (A.11)–(A.12). \square

Block structure. The Jacobian $J(\vartheta^*) \in \mathbb{R}^{D \times K}$ has $(F - 1)$ column blocks, one per free rule. Each block has $1 + d$ columns (intercept α_f plus slopes β_f). The derivative for rule f at menu A is nonzero only if f is active at A and belongs to $\mathcal{I}_i(A) \cup \mathcal{I}_{i_0}(A)$, i.e., f recommends either alternative i or the reference $i_0(A)$. Variation in which rules fall on which “side” across menus—i.e., rule switching—produces sign changes in the Jacobian entries, which tends to increase rank.

Binary environments as a special case When every menu has exactly two alternatives $A = \{L^1, L^2\}$, the log-ratio representation reduces to a single log-odds per menu:

$$\delta(A; \vartheta) = \log \frac{P(L^1 | A)}{P(L^2 | A)}.$$

Setting $i = L^1$ and $i_0 = L^2$, the recommending sets become $\mathcal{I}_{L^1}(A) = \mathcal{I}_L(A)$ and $\mathcal{I}_{L^2}(A) = \mathcal{I}_R(A)$ in the notation of the main text. The Jacobian entries (A.11)–(A.12) specialize to

$$\frac{\partial \delta(A)}{\partial \alpha_f} = \frac{s_f(A) \mathbf{1}\{f \in \mathcal{I}_L(A)\}}{S_L(A)} - \frac{s_f(A) \mathbf{1}\{f \in \mathcal{I}_R(A)\}}{S_R(A)},$$

where $S_L(A) = P(L^1 | A)$ and $S_R(A) = P(L^2 | A)$. Because $s_f(A)/S_L(A)$ is the within-left softmax share $s_{L,f}(A)$ in the main text and $s_f(A)/S_R(A)$ is $s_{R,f}(A)$, this recovers

$$\frac{\partial \delta(A)}{\partial \alpha_f} = s_{L,f}(A) - s_{R,f}(A), \quad \frac{\partial \delta(A)}{\partial \beta_f} = (s_{L,f}(A) - s_{R,f}(A)) \psi(A)^\top,$$

which is the binary specialization of the general Jacobian entries in Proposition A.3. The binary global identification result (Corollary 2) is the special case of Theorem A.1 obtained by setting $|A| = 2$.

Sources of identification. The closed-form Jacobian (A.11)–(A.12) makes the identification forces transparent. Three sources of variation contribute to rank:

- (i) *Side-switching*: a rule f recommends alternative i at some menus and alternative j at others. This produces sign changes in the Jacobian column for f , preventing collinearity with columns of rules that always recommend the same side.
- (ii) *Feature variation*: richer variation in $\psi(A)$ across menus generates more linearly independent rows in the Jacobian, even holding fixed which rules recommend which alternative.
- (iii) *Compositional variation*: changes in which rules are active across menus—so that the active-rule sets \mathcal{F}_A differ—alter the softmax shares $s_f(A)$ and the grouping structure, generating additional identifying variation.

Scope of the framework. The framework applies to any environment in which (a) a finite library of deterministic procedures and (b) an exogenous activity criterion can be defined. Natural applications beyond risky choice include intertemporal choice (where rules might be “choose the option with the highest present value at discount rate ρ ” and activity is determined by present-value dominance), allocation problems (where rules might correspond to equity or efficiency criteria and activity is determined by welfare dominance), and strategic settings (where rules are response heuristics and activity reflects rationalizability or dominance-based screening).

B Proof of Theorem 1 (fixed-feature identification)

Proof. Fix $x \in \mathbb{R}^d$ and let $\mathcal{A}_2(x) := \{A \in \mathcal{A}_2 : \psi(A) = x\}$. For each menu $A \in \mathcal{A}_2(x)$, define the odds ratio $r(A) := p(A)/(1 - p(A))$ and the column vector $h(A) \in \mathbb{R}^{|\mathcal{F}|}$ with entries $h_f(A) = \kappa_f^L(A) - r(A)\kappa_f^R(A)$. Denote the true weights by $\omega_f(x) = \exp(\alpha_f + \beta_f^\top x) > 0$.

Step 1 (from choice probabilities to linear restrictions). Under the CA-RRM the model-implied left-choice probability at menu A is

$$p(A) = \frac{\sum_f \kappa_f^L(A) \omega_f(x)}{\sum_f \kappa_f^L(A) \omega_f(x) + \sum_f \kappa_f^R(A) \omega_f(x)}.$$

Cross-multiplying $p(A) \sum_f \kappa_f^R(A) \omega_f(x) = (1 - p(A)) \sum_f \kappa_f^L(A) \omega_f(x)$ and dividing by $(1 - p(A))$ gives

$$\sum_{f \in \mathcal{F}} (\kappa_f^L(A) - r(A) \kappa_f^R(A)) \omega_f(x) = h(A)^\top \omega(x) = 0.$$

Since this holds for every $A \in \mathcal{A}_2(x)$, any vector in the cellwise identified set $\Omega(x)$ lies in the null space of the matrix $H(x)$ formed by stacking the rows $\{h(A)^\top : A \in \mathcal{A}_2(x)\}$.

Step 2 (sufficiency: rank $H(x) = |\mathcal{F}| - 1 \Rightarrow$ single ray). Suppose $\text{rank } H(x) = |\mathcal{F}| - 1$. Then $\ker H(x)$ is one-dimensional. Let v be a nonzero vector spanning this kernel. Because the true weights $\omega(x) \in \mathbb{R}_{++}^{|\mathcal{F}|}$ lie in $\Omega(x) \subseteq \ker H(x)$, we have $\omega(x) = cv$ for some scalar $c \neq 0$. Since $\omega(x)$ is strictly positive, v must be a scalar multiple of a strictly positive vector. Hence every $\tilde{\omega} \in \Omega(x)$ satisfies $\tilde{\omega} = c'v$ for some $c' > 0$, i.e. $\Omega(x) = \{c'\omega^*(x) : c' > 0\}$ is a single positive ray.

Step 3 (necessity: single ray \Rightarrow rank $H(x) = |\mathcal{F}| - 1$). We prove the contrapositive. Suppose $\text{rank } H(x) < |\mathcal{F}| - 1$. Then $\dim \ker H(x) \geq 2$. Pick two linearly independent vectors $v_1, v_2 \in \ker H(x)$ with $v_1 = \omega(x) \in \mathbb{R}_{++}^{|\mathcal{F}|}$. For all sufficiently small $\varepsilon > 0$, the vector $v_1 + \varepsilon v_2$ is also strictly positive (since v_1 has strictly positive entries). Moreover $v_1 + \varepsilon v_2 \in \ker H(x)$ by linearity. Therefore $v_1 + \varepsilon v_2 \in \Omega(x)$, and it is not proportional to v_1 (since v_1 and v_2 are linearly independent), so $\Omega(x)$ is not a single ray.

Step 4 (point identification under normalization). Normalizing $\omega_{f_0}(x) = 1$ restricts $\Omega(x)$ to the hyperplane $\{\omega : \omega_{f_0} = 1\}$. A single positive ray intersects this hyperplane in a unique point, so the normalization converts ray identification into point identification. \square

C Proof of Corollary 2 (detailed version)

Proof. Fix any menu A and write $x = \psi(A)$. Define the positive rule weights

$$\omega_f(x) := \exp(\alpha_f + \beta_f^\top x), \quad f \in \mathcal{F},$$

and let $\kappa_f^L(A) = \mathbf{1}\{f \in \mathcal{I}_L(A)\}$ and $\kappa_f^R(A) = \mathbf{1}\{f \in \mathcal{I}_R(A)\}$ denote whether rule f is decisive for the left or right option at A .

Step 1 (from choice probabilities to linear equations). Under the CA-RRM, the model-implied probability of choosing left at menu A is

$$p(A) = \frac{\sum_{f \in \mathcal{F}} \kappa_f^L(A) \omega_f(x)}{\sum_{f \in \mathcal{F}} \kappa_f^L(A) \omega_f(x) + \sum_{f \in \mathcal{F}} \kappa_f^R(A) \omega_f(x)}. \quad (\text{A.13})$$

Because $p(A) \in (0, 1)$, the odds ratio

$$r(A) := \frac{p(A)}{1 - p(A)} \in (0, \infty)$$

is well-defined. Using (A.13), the odds can be written as

$$r(A) = \frac{\sum_f \kappa_f^L(A) \omega_f(x)}{\sum_f \kappa_f^R(A) \omega_f(x)}.$$

Cross-multiplying yields

$$\sum_f \kappa_f^L(A) \omega_f(x) = r(A) \sum_f \kappa_f^R(A) \omega_f(x),$$

and bringing all terms to the left-hand side gives the linear restriction

$$\sum_{f \in \mathcal{F}} \left(\kappa_f^L(A) - r(A) \kappa_f^R(A) \right) \omega_f(x) = 0. \quad (\text{A.14})$$

Define the row vector $h(A) \in \mathbb{R}^{|\mathcal{F}|}$ by

$$h_f(A) := \kappa_f^L(A) - r(A) \kappa_f^R(A),$$

so (A.14) can be written compactly as

$$h(A)^\top \omega(x) = 0, \quad (\text{A.15})$$

where $\omega(x) = (\omega_f(x))_{f \in \mathcal{F}}$.

Step 2 (identifying $\omega(x)$ at a fixed feature value up to scale). Fix $k \in \{0, \dots, d\}$ and consider the menus A_{k1}, \dots, A_{kM_k} that satisfy $\psi(A_{km}) = x^{(k)}$. Crucially, the gate depends on A only through $x = \psi(A)$, so all these menus share the *same* unknown weight vector $\omega(x^{(k)})$, while the decisive-side indicators (κ^L, κ^R) (and hence $h(A)$) may vary across menus even when x is fixed. Applying (A.15) to each menu and stacking the resulting equations gives

$$\begin{pmatrix} h(A_{k1})^\top \\ \vdots \\ h(A_{kM_k})^\top \end{pmatrix} \omega(x^{(k)}) = 0, \quad \text{i.e.} \quad H^{(k)} \omega(x^{(k)}) = 0.$$

By (G1), $\text{rank}(H^{(k)}) = |\mathcal{F}| - 1$, so the nullspace of $H^{(k)}$ is one-dimensional: there exists a nonzero vector $\bar{\omega}^{(k)}$ such that every solution to $H^{(k)}\omega = 0$ is of the form $\omega = c\bar{\omega}^{(k)}$ for some scalar c . The true weight vector $\omega(x^{(k)})$ is strictly positive and lies in this nullspace, so $\bar{\omega}^{(k)}$ may be oriented to be strictly positive (set $\bar{\omega}^{(k)} := \omega(x^{(k)})$). Every admissible solution—i.e., every $\omega \in \mathbb{R}_{++}^{|\mathcal{F}|}$ with $H^{(k)}\omega = 0$ —is then exactly a positive multiple $c\bar{\omega}^{(k)}$ with $c > 0$. Thus, the menus with $\psi(A) = x^{(k)}$ identify $\omega(x^{(k)})$ up to a positive multiplicative scale factor.

Step 3 (pinning down scale using the normalization). Under the normalization $(\alpha_{f_0}, \beta_{f_0}) = (0, 0)$ we have, for all x ,

$$\omega_{f_0}(x) = \exp(0 + 0^\top x) = 1.$$

In particular, $\omega_{f_0}(x^{(k)}) = 1$. Since every solution to $H^{(k)}\omega = 0$ equals $c\bar{\omega}^{(k)}$, imposing the single

restriction $\omega_{f_0} = 1$ pins down c uniquely:

$$1 = \omega_{f_0}(x^{(k)}) = c \bar{\omega}_{f_0}^{(k)} \quad \Rightarrow \quad c = \frac{1}{\bar{\omega}_{f_0}^{(k)}}.$$

Hence there is a unique solution to $H^{(k)}\omega = 0$ that satisfies $\omega_{f_0} = 1$, and therefore $\omega(x^{(k)})$ is uniquely identified for each k .

Step 4 (recovering (α_f, β_f) from identified weights across k). Fix any rule $f \in \mathcal{F}$. From the definition of $\omega_f(\cdot)$,

$$\log \omega_f(x^{(k)}) = \alpha_f + \beta_f^\top x^{(k)}, \quad k = 0, \dots, d.$$

Stacking these $(d + 1)$ equalities yields the linear system

$$\begin{pmatrix} \log \omega_f(x^{(0)}) \\ \vdots \\ \log \omega_f(x^{(d)}) \end{pmatrix} = \begin{pmatrix} 1 & (x^{(0)})^\top \\ \vdots & \vdots \\ 1 & (x^{(d)})^\top \end{pmatrix} \begin{pmatrix} \alpha_f \\ \beta_f \end{pmatrix} = X \begin{pmatrix} \alpha_f \\ \beta_f \end{pmatrix}.$$

Assumption (G2) states that the $(d + 1)$ feature vectors $x^{(0)}, \dots, x^{(d)}$ are *affinely independent*, equivalently that the augmented regressor matrix X has full rank; hence X is invertible. Therefore (α_f, β_f) is uniquely determined. Since f was arbitrary, this holds for all $f \in \mathcal{F}$, establishing global identification (up to the imposed normalization). \square

D Proof of Theorem 3

Proof. Let $J := |\mathcal{F}|$, and let the finite menu support be

$$\mathcal{M} = \{A_1, \dots, A_M\}.$$

Write

$$p_m := p(A_m), \quad r_m := \frac{p_m}{1 - p_m}, \quad m = 1, \dots, M.$$

For each menu A_m , define the sample share

$$\hat{p}_m := \frac{1}{n_m} \sum_{i=1}^{n_m} Y_{mi},$$

and let $\hat{r}_m = \hat{p}_m / (1 - \hat{p}_m)$, with the understanding that any trimming to $[\varepsilon_n, 1 - \varepsilon_n]$ is asymptotically inactive under (E1) because $\varepsilon_n \downarrow 0$.

For each identifying feature value $x^{(k)}$, let

$$\mathcal{M}_k = \{m_{k1}, \dots, m_{kM_k}\}$$

denote the menus in the k th cell, i.e. the menus satisfying $\psi(A_m) = x^{(k)}$. Define

$$\omega^{(k)} := \omega(x^{(k)}), \quad \omega^{(k)} = (1, \eta^{(k)\top})^\top,$$

where the normalization $\omega_{f_0}(x^{(k)}) = 1$ is imposed for every k .

We prove the three claims in turn.

Steps 1–2: Joint asymptotic normality of odds ratios.

For each menu m , \hat{p}_m is a sample mean of i.i.d. Bernoulli(p_m) variables. Because menu-specific samples are mutually independent across menus (by the sampling scheme) and the number of menus M is fixed, the multivariate CLT gives $\sqrt{N}(\hat{p} - p) \xrightarrow{d} \mathcal{N}(0, \Sigma_p)$, where $\Sigma_p := \text{diag}(p_m(1 - p_m)/\pi_m)$ and $\pi_m := \lim n_m/N$ by (E5). The diagonal structure of Σ_p reflects cross-menu independence. The delta method applied to the componentwise map $g(u) = u/(1 - u)$ (smooth under (E1)) yields

$$\sqrt{N}(\hat{r} - r) \xrightarrow{d} \mathcal{N}(0, \Sigma_r), \quad \Sigma_r = \text{diag}\left(\frac{p_m}{\pi_m(1 - p_m)^3}\right). \quad (\text{A.16})$$

Trimming to $[\varepsilon_n, 1 - \varepsilon_n]$ is asymptotically inactive under (E1).

Step 3: From odds ratios to the restriction matrix $H^{(k)}$.

Fix a cell k . Recall that the (m, f) entry of $H^{(k)}$ is $h_f(A_m) = \kappa_f^L(A_m) - r_m \kappa_f^R(A_m)$. The decisive-side indicators κ_f^L, κ_f^R are deterministic functions of the menu, so $H^{(k)}$ depends on the data only through the odds ratios $r^{(k)} = (r_{k1}, \dots, r_{kM_k})^\top$, and does so affinely: there exists a deterministic matrix B_k (constructed from the stacked indicators) such that $\text{vec}(\hat{H}^{(k)} - H^{(k)}) = B_k(\hat{r}^{(k)} - r^{(k)})$. Because this map is linear, the CLT for the odds ratios (A.16) carries over directly:

$$\sqrt{N} \text{vec}(\hat{H}^{(k)} - H^{(k)}) \xrightarrow{d} \mathcal{N}(0, \Sigma_H^{(k)}), \quad \Sigma_H^{(k)} := B_k \Sigma_r^{(k)} B_k^\top.$$

Step 4: Cellwise weight recovery.

Partition $H^{(k)} = [h_0^{(k)} \quad H_-^{(k)}]$ where the first column corresponds to the baseline rule f_0 . The normalization $\omega_{f_0} = 1$ and the linear restriction $H^{(k)}\omega^{(k)} = 0$ together imply $H_-^{(k)}\eta^{(k)} = -h_0^{(k)}$, where $\eta^{(k)} = (\omega_f(x^{(k)}))_{f \neq f_0}$ collects the non-baseline weights. Under (E2), $\text{rank } H^{(k)} = J - 1$, so the null space of $H^{(k)}$ is one-dimensional (by Theorem 1). This implies $H_-^{(k)}$ has full column rank $J - 1$: if it did not, $\ker H^{(k)}$ would contain a vector with $\omega_{f_0} = 0$ in addition to the true $\omega^{(k)}$, giving dimension ≥ 2 . The least-squares map

$$\phi_k(H) := -(H_-^\top H_-)^{-1} H_-^\top h_0$$

is therefore well-defined and smooth in a neighborhood of $H^{(k)}$ (since the Gram matrix $H^\top H_-$ is nonsingular and matrix inversion is smooth). The delta method applied to $\hat{\eta}^{(k)} = \phi_k(\hat{H}^{(k)})$ yields

$$\sqrt{N}(\hat{\eta}^{(k)} - \eta^{(k)}) \xrightarrow{d} \mathcal{N}(0, V_\eta^{(k)}), \quad V_\eta^{(k)} = D\phi_k(H^{(k)}) \Sigma_H^{(k)} D\phi_k(H^{(k)})^\top,$$

where $D\phi_k$ denotes the Jacobian of ϕ_k with respect to $\text{vec}(H)$. Embedding via $\hat{\omega}^{(k)} = (1, \hat{\eta}^{(k)\top})^\top$ gives $\sqrt{N}(\hat{\omega}^{(k)} - \omega^{(k)}) \xrightarrow{d} \mathcal{N}(0, V_\omega^{(k)})$, where $V_\omega^{(k)}$ is a $J \times J$ matrix obtained from $V_\eta^{(k)}$ by inserting a zero row and column in the f_0 position. This reflects the normalization $\omega_{f_0} \equiv 1$: the baseline weight is not estimated but fixed, so $\hat{\omega}_{f_0}^{(k)} - \omega_{f_0}^{(k)} = 0$ with probability one and the f_0 coordinate contributes zero variance.

Step 5: Log-weight transformation and stacking across cells.

For each non-baseline rule f and cell k , define $\hat{y}_f^{(k)} := \log \hat{\omega}_f(x^{(k)})$ and $y_f^{(k)} := \log \omega_f(x^{(k)})$. Assumption (E4) ensures $\omega_f(x^{(k)}) \geq \underline{\omega} > 0$, so the logarithm is smooth at the truth and the delta method gives

$$\sqrt{N}(\hat{y}_f^{(k)} - y_f^{(k)}) \xrightarrow{d} \mathcal{N}(0, V_{y,f}^{(k)}), \quad V_{y,f}^{(k)} = \omega_f(x^{(k)})^{-2} e_f^\top V_\omega^{(k)} e_f.$$

To see this, note that $\hat{y}_f^{(k)} = g(\hat{\omega}^{(k)})$ where $g(\omega) = \log \omega_f$ depends only on the f -th coordinate. The gradient is $\nabla g(\omega) = e_f / \omega_f$, where e_f is the f -th standard basis vector. The delta method gives asymptotic variance $\nabla g^\top V_\omega^{(k)} \nabla g = \omega_f(x^{(k)})^{-2} e_f^\top V_\omega^{(k)} e_f$. The quadratic form $e_f^\top V_\omega^{(k)} e_f$ is simply the (f, f) diagonal entry of $V_\omega^{(k)}$, i.e. the asymptotic variance of the f -th weight estimator $\hat{\omega}_f^{(k)}$ in that cell.

Stacking across cells $k = 1, \dots, K$, the joint CLT for $\hat{y}_f := (\hat{y}_f^{(1)}, \dots, \hat{y}_f^{(K)})^\top$ is

$$\sqrt{N}(\hat{y}_f - y_f) \xrightarrow{d} \mathcal{N}(0, V_{y,f}), \quad V_{y,f} = \text{diag}(V_{y,f}^{(1)}, \dots, V_{y,f}^{(K)}).$$

The diagonal structure holds because the cells partition the menus into disjoint groups with independent within-menu samples, so the first-stage estimators from distinct cells are asymptotically independent. This completes part (i).

Step 6: Second-stage asymptotics for the affine parameters.

Fix $f \neq f_0$. By construction $y_f = X_K \gamma_f$ where $\gamma_f = (\alpha_f, \beta_f^\top)^\top$ and X_K stacks the augmented cell centroids $z_k = (1, x^{(k)\top})^\top$. Let $A_f := (X_K^\top W_f X_K)^{-1} X_K^\top W_f$, which is nonsingular by (E3). Then $\hat{\gamma}_f - \gamma_f = A_f(\hat{y}_f - y_f)$, so

$$\sqrt{N}(\hat{\gamma}_f - \gamma_f) \xrightarrow{d} \mathcal{N}(0, V_{\gamma,f}), \quad V_{\gamma,f} = A_f V_{y,f} A_f^\top.$$

This proves part (ii).

Step 7: Functionals of the gate parameters.

Let $\theta = \{\gamma_f\}_{f \neq f_0}$ be the stacked parameter vector. By part (ii), $\sqrt{N}(\hat{\theta} - \theta_0) \xrightarrow{d} \mathcal{N}(0, V_\theta)$. For any continuously differentiable functional τ , the delta method gives $\sqrt{N}(\tau(\hat{\theta}) - \tau(\theta_0)) \xrightarrow{d} \mathcal{N}(0, \nabla\tau(\theta_0)^\top V_\theta \nabla\tau(\theta_0))$, proving part (iii). \square

E Attention-Rule Removal

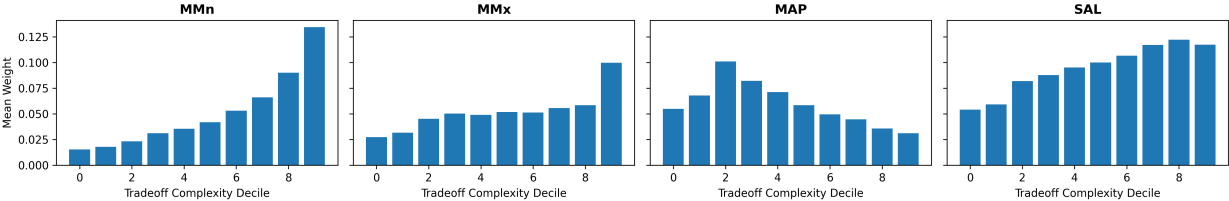
Table A.1 replicates the main cross-validation comparison (Table 3) with the rule-gating model restricted to the 10 economic rules (excluding A1/A2).

Table A.1: Robustness: predictive performance after removing attention defaults A1/A2. Rule-gating (10 rules) excludes the two attention defaults; all other models are identical to Table 3.

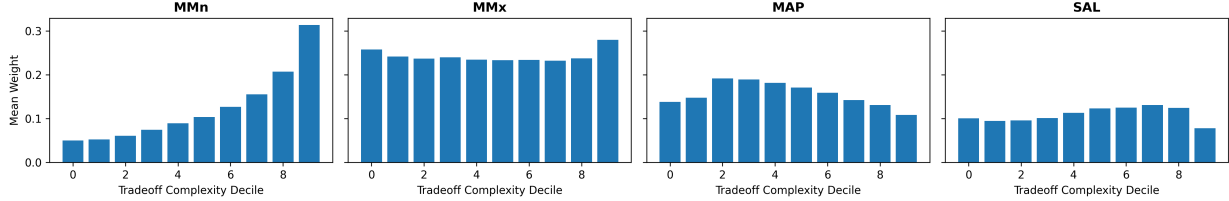
Model	Mean MSE	SD	Mean MSE _w	Best LR
MOT [†]	0.01139	0.00056	n.a.	0.001
Rule-gating	0.01168	0.00049	0.01155	0.010
Context-dependent	0.01344	0.00081	0.01330	0.010
Value-based	0.01921	0.00081	0.01904	0.010
Rule-gating (Spec A)	0.02014	0.00092	0.01999	0.010
Neural PT	0.02064	0.00085	0.02050	0.010
Neural CPT	0.02145	0.00093	0.02134	0.010
Neural EU	0.02215	0.00085	0.02205	0.010

Note: [†]MOT learning rate is selected by test MSE following the published protocol of Peterson et al. (2021). Rule-gating (Spec A) excludes A1/A2. The full 12-rule specification (Rule-gating) is reproduced from Table 3 for comparison.

Figures A.1 and A.2 replicate the complexity and risk mechanism plots under the 10-rule specification. The qualitative patterns persist: removing A1/A2 reallocates mass to the structured rules, but directional movements are unchanged.

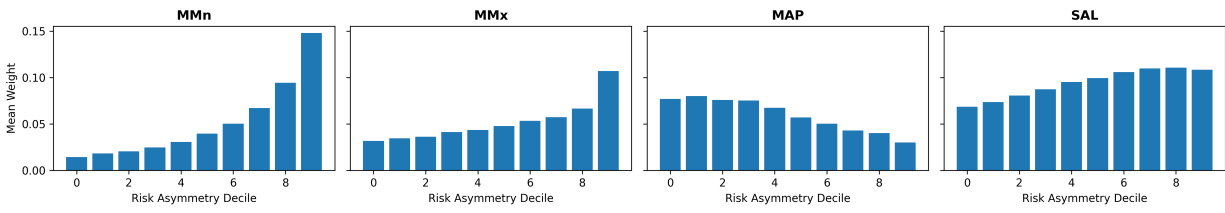


(a) Full library (12 rules).

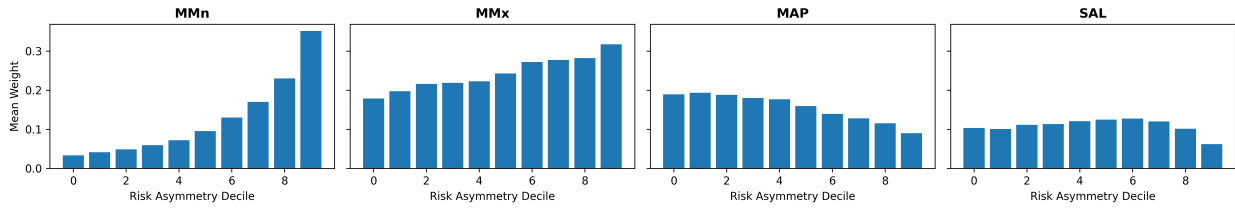


(b) 10 rules (no A1/A2).

Figure A.1: Mean effective responsibility weights across deciles of tradeoff complexity for MMN, MMx, MAP, SAL: full library vs. 10-rule specification.



(a) Full library (12 rules).



(b) 10 rules (no A1/A2).

Figure A.2: Mean effective responsibility weights across deciles of risk asymmetry for MMN, MMx, MAP, SAL: full library vs. 10-rule specification.

F Latent Gate vs. Effective Responsibility Weights

Figures A.3 and A.4 compare the effective (CA-normalized) responsibility weights $\tilde{q}_f(A; \theta)$ with the latent gate outputs $q_f(A; \theta)$ across deciles of tradeoff complexity and risk asymmetry. For each rule, the top panel shows the effective weight (as plotted in Figures 5–6) and the bottom panel shows the corresponding latent gate propensity before conditioning on activity. The qualitative patterns are preserved: for example, MMX rises with complexity and MAP declines under both measures. This confirms that the comparative-statics patterns in the main text reflect genuine variation in the learned gate, not mechanical artifacts of the activity normalization.

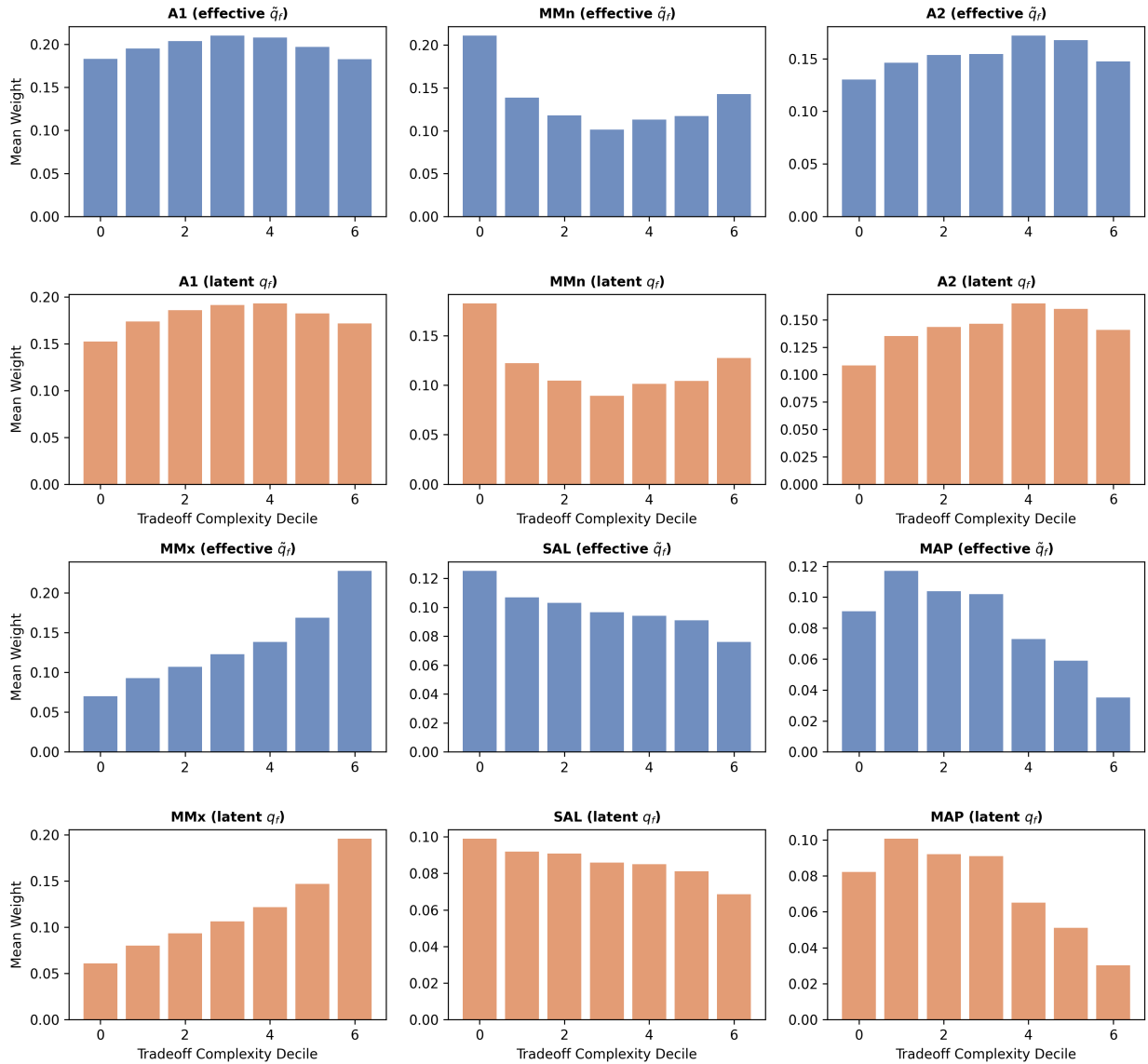


Figure A.3: Effective responsibility weight \tilde{q}_f (top, blue) vs. latent gate output q_f (bottom, orange) across deciles of tradeoff complexity, for the six highest-weight rules.

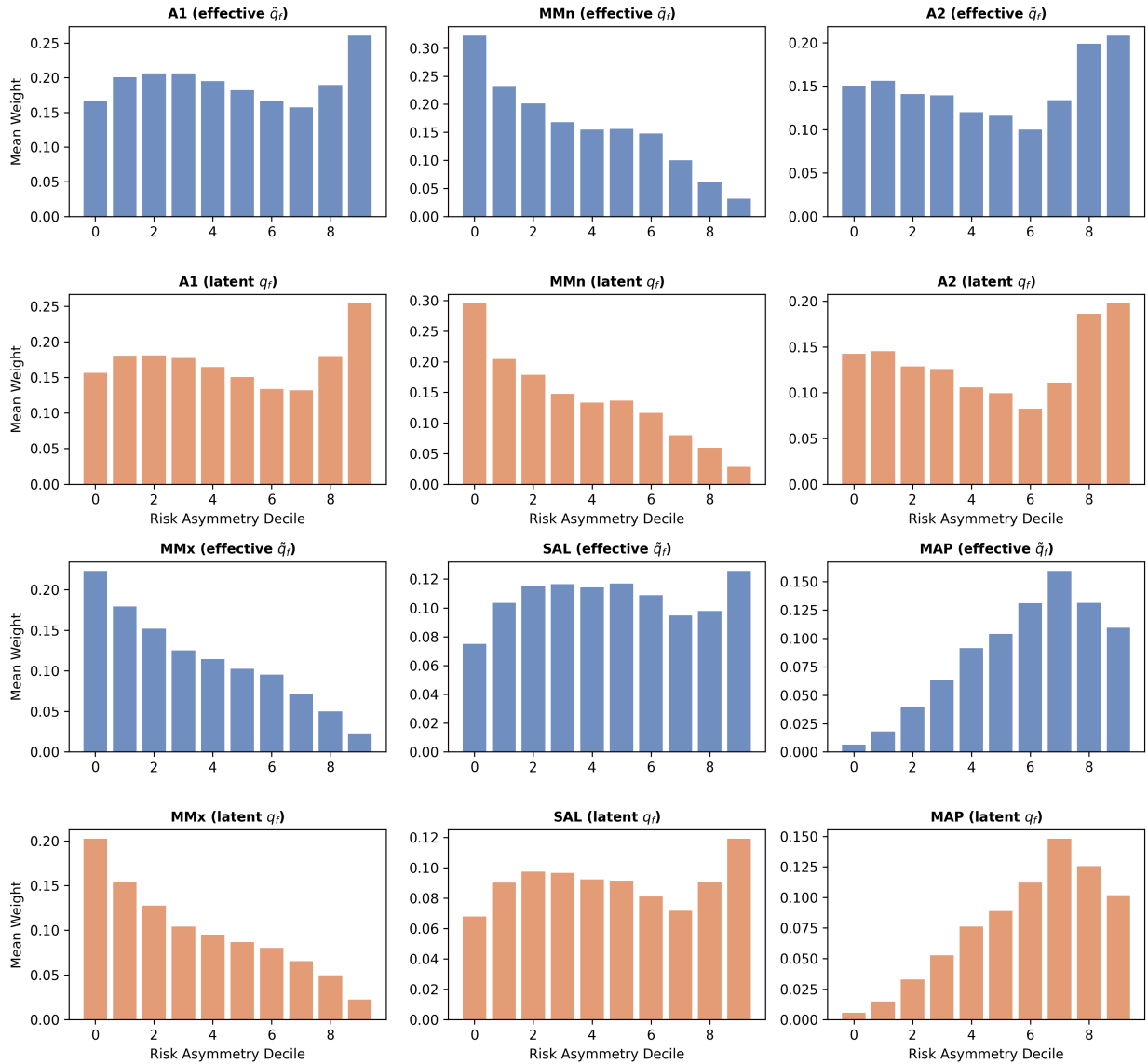


Figure A.4: Effective responsibility weight \tilde{q}_f (top, blue) vs. latent gate output q_f (bottom, orange) across deciles of risk asymmetry, for the six highest-weight rules.

Table A.2: Paired comparisons of models against the rule-gating model (fold-level deltas). Positive delta means the comparison model performs worse. SE is split-to-split standard error.

Model A	vs.	Metric	Mean delta	SE	N folds
Context-dependent	Rule-gating	test_mse	-0.00045	0.00010	50
Neural CPT	Rule-gating	test_mse	0.00756	0.00014	50
Neural EU	Rule-gating	test_mse	0.00826	0.00012	50
Neural PT	Rule-gating	test_mse	0.00675	0.00013	50
Rule-gating	Rule-gating	test_mse	-0.00221	0.00006	50
Value-based	Rule-gating	test_mse	0.00532	0.00012	50
MOT	Rule-gating	test_mse	-0.00250	0.00012	50

G Paired Comparisons

Table A.2 reports split-level comparisons for out-of-sample performance. For each pair of models, we compute the per-split difference in test MSE and report the mean and standard error across the 50 random splits. Because the train/test splits overlap across repetitions, these standard errors should be interpreted as descriptive measures of split-to-split variability rather than formal sampling-based inference.

H Model-Level Uncertainty Intervals

Table A.3 reports split-variability intervals ($\text{mean} \pm 1.96 \times \text{SE}$) for each model’s out-of-sample metrics, constructed from fold-to-fold variability across the 50 CV splits. These intervals are descriptive summaries of how performance varies across train/test partitions, not formal confidence intervals.

Table A.3: Model-level split-variability intervals from fold-to-fold variability (50 splits).

Model	Mean MSE	SE	CI low	CI high
MOT	0.01139	0.00008	0.01124	0.01155
Rule-gating	0.01168	0.00007	0.01154	0.01182
Context-dependent	0.01344	0.00012	0.01322	0.01367
Value-based	0.01921	0.00011	0.01898	0.01943
Neural PT	0.02064	0.00012	0.02040	0.02087
Neural CPT	0.02145	0.00013	0.02119	0.02171
Neural EU	0.02215	0.00012	0.02192	0.02239

Note: Intervals computed as $\text{mean} \pm 1.96 \times \text{SE}$, where $\text{SE} = \text{SD} / \sqrt{n_{\text{folds}}}$. These are descriptive split-variability intervals, not formal confidence intervals.

I Ablation Effect Split-Variability Intervals

Table A.4 reports split-variability intervals for the absolute ablation effect $\Delta\text{MSE} = \text{MSE}^{-f} - \text{MSE}^{\text{full}}$, constructed from fold-to-fold variability. For each rule f , we compute the per-fold MSE increase from dropping rule f from the full 12-rule library, then report the mean, standard error, and interval bounds. (The relative index $\phi(f) = \Delta\text{MSE}/\text{MSE}^{\text{full}}$, as defined in Equation (16), is reported in Table A.5.)

The leading ablation effects are SAL2 and SAL, followed by REGMED and REG. At the other extreme, MMA has a small negative ablation effect (removing it slightly improves MSE), indicating that its contribution is fully substitutable by the remaining rules.

Table A.4: Ablation effect (absolute MSE change) with split-variability intervals from fold-to-fold variability. Each rule is ablated from the full 12-rule library.

Rule	Mean ΔMSE	SE	CI low	CI high
SAL2	0.00061	0.00005	0.00051	0.00071
SAL	0.00054	0.00004	0.00046	0.00063
REGMED	0.00021	0.00003	0.00014	0.00028
REG	0.00014	0.00005	0.00005	0.00023
MAP	0.00014	0.00003	0.00007	0.00020
MMX	0.00013	0.00004	0.00005	0.00022
MMN	0.00011	0.00003	0.00005	0.00017
DIS	0.00005	0.00003	-0.00001	0.00010
DISMED	0.00000	0.00003	-0.00006	0.00006
MMA	-0.00004	0.00003	-0.00009	0.00001

Note: $\Delta\text{MSE} = \text{MSE}^{-f} - \text{MSE}^{\text{full}}$: absolute MSE increase when rule f is dropped (fold-level paired differences). The relative index $\phi(f) = \Delta\text{MSE}/\text{MSE}^{\text{full}}$ is reported in Table A.5.

J Decomposition Stability

Table A.5 reports the stability of the responsibility weights w_f and ablation index $\phi(f)$ across the 50 CV folds. For each rule, we report the mean, standard deviation, and coefficient of variation ($\text{CV} = \text{SD}/\text{mean}$) across folds. The Spearman rank correlations reported in the table note summarize the stability of the *orderings*: for all $\binom{50}{2}$ fold pairs, we compute the Spearman correlation between the fold-level w_f (or $\phi(f)$) vectors, and report the mean, minimum, and maximum.

K Selection Stability

Table A.6 reports the frequency with which each behavioral rule is selected in the top- k set across the 50 cross-fitted CV folds. Higher frequency indicates more stable selection.

Table A.5: Decomposition stability across 50 CV folds. For each rule f : mean, standard deviation, and coefficient of variation (CV) of the responsibility weight w_f and ablation index $\phi(f)$ across folds.

Rule	Mean w_f	SD w_f	CV w_f	Mean $\phi(f)$	SD $\phi(f)$	CV $\phi(f)$
A1	0.2882	0.0098	0.03	—	—	—
A2	0.2631	0.0092	0.03	—	—	—
SAL	0.0927	0.0060	0.06	0.0471	0.0271	0.57
REG	0.0717	0.0056	0.08	0.0123	0.0270	2.19
MAP	0.0595	0.0047	0.08	0.0119	0.0193	1.62
MMX	0.0500	0.0058	0.12	0.0118	0.0263	2.23
MMN	0.0432	0.0143	0.33	0.0095	0.0177	1.86
SAL2	0.0385	0.0022	0.06	0.0529	0.0300	0.57
REGMED	0.0373	0.0085	0.23	0.0178	0.0210	1.18
DISMED	0.0268	0.0076	0.28	0.0005	0.0179	39.76
DIS	0.0218	0.0104	0.48	0.0041	0.0174	4.28
MMA	0.0073	0.0048	0.65	-0.0032	0.0157	4.98

Note: Spearman rank correlation of w_f orderings across all fold pairs: mean $\rho = 0.930$, range $[0.762, 1.000]$.
Spearman rank correlation of $\phi(f)$ orderings: mean $\rho = 0.442$, range $[-0.636, 0.952]$.

Table A.6: Cross-fitted selection stability: frequency of each behavioral rule appearing in top- k across 50 folds.

Rule	Freq. top-3	Freq. top-5	Freq. top-7	Freq. top-12
A1	1.00	1.00	1.00	1.00
A2	1.00	1.00	1.00	1.00
DIS	0.00	0.00	0.00	1.00
DISMED	0.00	0.00	0.00	1.00
MAP	0.00	0.96	1.00	1.00
MMA	0.00	0.00	0.00	1.00
MMN	0.00	0.00	0.00	1.00
MMX	0.00	0.04	1.00	1.00
REG	0.00	1.00	1.00	1.00
REGMED	0.00	0.00	0.44	1.00
SAL	1.00	1.00	1.00	1.00
SAL2	0.00	0.00	0.56	1.00

Note: Frequency 1.00 means the rule is selected in every fold.

L Feature-Based Baselines

We train two baseline models—a *fractional logit* (Papke and Wooldridge, 1996) and a *gradient-boosted tree ensemble* (GBT, scikit-learn)—on three feature sets: (F1) summary statistics (≈ 18 dim), (F2) rule indicators (24 dim), and (F3) concatenation (≈ 42 dim). All use the same 50-fold

Table A.7: Feature-based baselines: out-of-sample MSE (50 splits). Rules = binary rule indicators; Stats = lottery summary statistics; Combined = concatenation.

Model	Mean MSE	SD	Mean MSE _w	Features
GBT (combined)	0.00957	0.00041	0.00947	F3
GBT (stats)	0.00997	0.00041	0.00986	F1
Fractional logit (combined)	0.01579	0.00073	0.01565	F3
GBT (rules)	0.02039	0.00079	0.02013	F2
Fractional logit (rules)	0.02346	0.00103	0.02324	F2
Fractional logit (stats)	0.02362	0.00099	0.02338	F1

Note: F1 = summary statistics (≈ 18 dim); F2 = rule indicators (24 dim); F3 = combined (≈ 42 dim). All models use the same 50-fold CV protocol as Table 3.

CV protocol. The fractional logit is a binomial GLM with logit link on the continuous choice frequency $\hat{p}(A) \in [0, 1]$; L_2 regularization is selected from $\{0, 0.01, 0.1, 1\}$ by inner-fold validation. GBT uses `max_depth=4` with the number of estimators selected from $\{100, 200, 500\}$.

Results. Table A.7 reports results. On rule features alone (F2), rule-gating substantially outperforms both baselines. This comparison isolates the gating mechanism’s contribution (not a pure feature comparison, since rule-gating also uses $z(A)$). GBT on combined features (F3) outperforms all structured models but provides no behavioral decomposition.

M Placebo Rule Library

We construct a placebo test by randomly reassigning each rule’s $(L_f(A), A_f(A))$ pairs across menus within 10 complexity strata,¹⁴ preserving marginal statistics but destroying menu-specific content (50 repetitions). Table A.8 shows that the placebo library produces substantially higher MSE, confirming that the rule indicators carry genuine, menu-specific predictive content.

N Raw-Encoding Gate Benchmark

We estimate a variant using the raw encoding $\psi(A) \in \mathbb{R}^{40}$ instead of $z(A)$, yielding $40 \times |\mathcal{F}|$ gate parameters. The raw-encoding gate achieves MSE 0.0139 vs. 0.0117 for the baseline—about 19% worse (Figure A.5)—indicating that the interpretable summary statistics capture decision-relevant variation without the overfitting induced by higher-dimensional inputs.

¹⁴Stratified by support-count quantiles to preserve marginal activity rates per stratum.

Table A.8: Placebo rule library test. The “Real” row reports the rule-gating model with the actual rule indicators; the “Placebo” row uses stratified-permuted indicators that preserve marginal activity rates per rule per complexity bin but destroy the menu-to-indicator mapping.

Library	Mean MSE	SD	n
Real (rule-gating)	0.01168	0.00049	50
Placebo (permuted)	0.02197	0.00032	50

Note: Placebo indicators are constructed by independently permuting each rule’s (L_f, A_f) pairs across menus within quantile bins of menu complexity (number of nonzero outcomes). The gate architecture, training protocol, and all other inputs are identical to the main rule-gating model. SD for the real model is across 50 CV folds; SD for the placebo is across permutations.

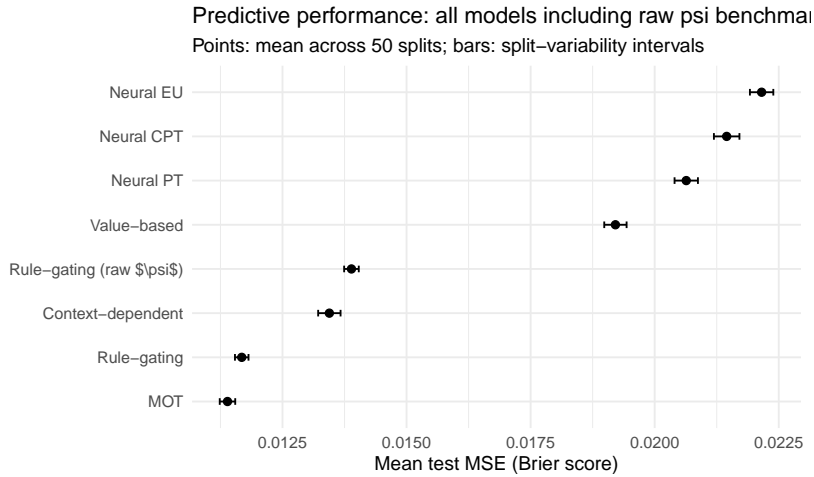


Figure A.5: Predictive performance of all models including the raw-encoding gate variant: mean test MSE across 50 random splits with split-variability intervals.

O Local Identification for High-Dimensional Gate Features

The global conditions (G1)–(G2) require within-feature replication, which fails when the gate operates on the essentially injective raw encoding $\psi(A) \in \mathbb{R}^{4M}$. For such specifications, identification is assessed locally via Theorem A.2: if the Jacobian $J(\vartheta^*)$ of the identification map (Section A.9) has full column rank at the fitted parameters, part (a) guarantees local identification.

In Section 7.1, both diagnostics support identification: the global conditions hold for the $z(A)$ specification, and the Jacobian achieves full column rank at the fitted parameters for both the $z(A)$ and raw- ψ specifications, where “full column rank” is evaluated relative to the effective parameter dimension (accounting for the redundancy in $z(A)$ that reduces its dimension from 12 to $d_{\text{eff}} = 11$).